STUDIES ON ABATEMENT OF FLUORIDES USING FLUIDIZED BED REACTOR: ASPEN PLUS SIMULATION

A Thesis Submitted to the

National Institute of Technology, Rourkela

In Partial Fulfillment for the Requirements

Of

Master of Technology (By Research) Degree

In

CHEMICAL ENGINEERING

By

Mr. Harjeet Nath

Roll No. 612CH3002

Under the guidance of

Dr. (Mrs.) Abanti Sahoo

Department of Chemical Engineering
National Institute of Technology
Rourkela-769008

CERTIFICATE

This is to certify that M.Tech. (Research) thesis entitled, "S**tudies on abatement of Fluorides using Fluidized Bed Reactor : ASPEN PLUS Simulation**" submitted by **Mr. Harjeet Nath** in partial fulfillments for the requirements of the award of Master of Technology (Research) degree in Chemical Engineering at National Institute of Technology, Rourkela is an authentic work carried out by him under my supervision and guidance. He has fulfilled all the prescribed requirements and the thesis, which is based on candidate's own work, has not been submitted elsewhere.

Supervisor
Dr. (Mrs.) Abanti Sahoo
Department of Chemical Engineering,
National Institute of Technology,
Rourkela - 769008,
Orissa

ACKNOWLEDGEMENTS

I feel immense pleasure and privilege to express my deep sense of gratitude and feel indebted towards all those people who have helped, inspired and encouraged me during the preparation of this report.

I am grateful to my supervisor, **Prof. Abanti Sahoo**, for her kind support, guidance and encouragement throughout the project work, also for introducing me to this topic.

I express my gratitude and indebtedness to Dr. Sujit Sen, Dr. Pradip Choudhury and Dr. Ramakar Jha for their valuable suggestions and instructions at various stages of the work.

I would also like to thank HOD, **Prof. Pradip Rath** for his kind help to make this report complete. I am also thankful to all the staff and faculty members of Chemical Engineering Department, National Institute of Technology, Rourkela for their consistent encouragement.

I would also like to extend my sincere thanks to my seniors especially to Ms. Pranati Sahoo and Ms. Subhasini Jena and my friends Mr. Praneeth Rao, Mr. Ujjal Mondal and Mr. Suresh Allauwaswamy for their unconditional assistance and support.

Last but not the least; I would like to thank whole heartedly my parents and family members whose love and unconditional support, both on academic and personal front, enabled me to see the light of this day.

Thanking You,

HARJEET NATH
Roll No. 612CH3002

CONTENTS

LIST OF TABLES

LIST OF FIGURES

ABSTRACT

A Fluidized Bed Reactor (FBR) is designed to be used for operating temperature till 500^0C. Attempt has been made to treat the gaseous effluents of Aluminum industry for abatement of Fluorides using FBR. Red Mud (RM) is used as the bed material. Air is used as the Fluidizing medium and the gaseous effluent is fed as the secondary fluid. Bed material (RM) is analyzed before the experiments. The Hydrodynamics and the reaction results of the FBR are studied using Aspen Plus v8.4 simulation software package. The fluidization velocity, TDH, solids holdup, surface area, distributor pressure drop, bottom zone pressure drop, freeboard pressure drop, fluidized bed pressure drop, overall pressure drop and the change in the amount of reactants and the amount of product formed are evaluated from the simulation package. The phase composition and structural transition of the bed materials fluidized at different temperatures are investigated after the experiment. The presence of components such as AlF_3, FeF_2, FeF_3 and NaF in the bed material confirmed the abatement of Fluorides from the gaseous effluents. The simulated results obtained from the ASPEN PLUS Simulation software package indicated the reduction of Fluorides from the gaseous effluents by approx. 25 % .The simulated results are compared with the experimental results . This method of fluoride abatement can be very much effective for those industries where fluoride level is a point of concern.

Keywords: Aspen Plus, Fluidized Bed Reactor, Fluoride Abatement, Geldart A Particles

CHAPTER – 1

INTRODUCTION

1.1 Abatement of Fluorides

There has been an enormous expansion in the use of fluorine compounds in agriculture and industry over the past decade. People are exposed to airborne fluorides because of air pollution caused by aluminum smelting, phosphatic fertilizer, petroleum refining, glass and semi-conductor chips manufacturing industries. Exposure to fluoride gas either in the form of direct contact or inhalation with the skin leads to serious health hazards. Fluorides can lead to serious health hazards even at very low concentrations. Industrial fluorides are mostly released in the form of hydrogen fluoride (HF), Sodium Fluoride (NaF) and Calcium Fluorides (CaF_2).

Atomic Fluorine and molecular Fluorine are used for plasma etching in semiconductor manufacturing, flat panel display production etc. Fluorine is indirectly used in the production of low plastics such as Teflon and in halons such as Freon, in the production of uranium. Fluoro-chloro hydrocarbons are used extensively in the air conditioning and in refrigeration. Fluorides are often used in toothpaste and somewhat controversially, to municipal water supplies to prevent dental cavities. In addition to it, various phosphatic fertilizers and petroleum industries emit Fluorine to the atmosphere.

Fluorine values useful to our body are very close to toxic values, so a dispense not aimed and personalized can cause high risk of overdosing and chronicle poisoning, with consequent skeletal deformation, spots on tooth enamel, osteosclerosis, neurological disorders, damages on the thyroids and even tumors. This gas is very dangerous as it can

cause death at moderately high concentrations. At low concentrations it can cause eye and nose irritations. Its exposure as little as 1 ppm can prove to be very fatal and that too it's very difficult to breakdown or reduce to non-toxic forms. Therefore it is highly desirable to minimize the concentration of such harmful gases and by-products present in the environment. There is also a need to reduce the harmful content of the effluents gas released into the atmosphere in a very efficient and inexpensive manner in order to protect vegetation and grazing animals and therefore human health. Recently, the strict restrictions from the Ministry of Environment and Forests, Govt. of India on the emission of harmful fluoride containing gases into the atmosphere have increased the need of impurity free effluents gas. Thus all the industries which emit such fluoride containing gases should adopt modern abatement techniques to reduce their emissions in order to meet the Govt. regulations.

The most recent abatement technique for fluoride includes the Fluidized Bed method. This study focusses on fluidized bed technology for the abatement of Fluorides from gaseous effluents of Aluminum Industry.

1.2 Fluidized Bed Technology

Fluidization is the phenomenon of imparting the properties of a fluid to a bed of particulate solids by passing a fluid through the bed at a velocity which brings the fixed or static bed to its loosest possible state just before its transformation into a fluid like bed. Fluidized bed is widely used in different industries. Fluidized Bed Technology has several advantages of other technologies.

1.2.1 Advantages

Some of the advantages of using a FBR is as follows:

- Good fluid-solid contact.
- A high rate of heat and mass transfer under isothermal operating conditions.
- A fluid like behavior facilitates the circulation between two adjacent reactors (e.g. catalytic cracking and regeneration combination).
- There is no moving part, and hence a fluidized bed reactor is not a mechanically agitated reactor. For this reason, maintenance costs can be low.
- The reactor is mounted vertically and thus saves space. This aspect is particularly important for a plant located at a site where land cost is high.
- A continuous process coupled with high throughput is possible.
- The fluidized bed is suitable for accomplishing heat-sensitive or exothermic or endothermic reactions.
- The system offers ease of control even for large scale operation.
- Excellent heat transfer within fluidized bed makes it possible to be used as low surface area heat exchangers inside the bed.
- Multistage operations are possible, and hence the solids residence time as well as the fluid resistance time can be adjusted to desired levels.

1.2.2 Applications

FBR has extensive industrial applications due to above mentioned advantages. It is used in nuclear power plants, chemical, biochemical and metallurgy industry. It is extensively used in Petroleum industry for fluid bed catalytic cracking, in chemical operations i.e.

gasification and carbonization of coal, roasting of sulphur ores, reduction of iron oxides, blending of granular materials, granulation of fertilizer, combustion, incineration, and pyrolysis and in physical operations i.e. drying of solids such as crushed minerals, sand, polymers, pharmaceuticals, fertilizers and crystalline products, coating of metals with plastic and particles in pharmaceutical and agricultural industries, for transportation, granulation of solids, heating, cooling and water & waste treatment etc. The commercial applications of fluidization are fluid catalytic cracking, reforming, Fischer-Tropsch synthesis, catalyst regeneration, granulation (growing particles), oxidation reactions involving solid catalyzed gas phase reactions, fluid coking, bio-oxidation process for waste water treatment and transportation of solids like slurry pipeline for coal.

1.3 ASPEN PLUS Simulation

ASPEN was developed first at the Massachusetts Institute of Technology (MIT) under a project of Department of Energy, United States to simulate coal conversion processes. It has now become a powerful tool for engineers to model chemical, power generation and other processes. The ASPEN PLUS process simulator has been used by different investigators to simulate coal conversion with the examples including methanol synthesis, integrated coal liquefaction process, integrated coal gasification combined cycle power plants, atmospheric fluidized bed combustor processes, and coal gasification simulation. ASPEN PLUS provides customers with a complete set of unit operation model to simulate the process of operation, from a single operation unit to the entire process simulation. Until 2012 researchers were using a combination of various user defined models to represent the FBR. Due to the unavailability of a predefined FBR, their hydrodynamic studies were not possible. By the end of 2013, ASPEN PLUS package

included a FBR where the bed hydrodynamics can be studied which provided the researchers a brief description about the working of a FBR. The current version of the ASPEN PLUS Package (V8.4) includes the reactions taking place inside the FBR where reaction kinetics data plays the major role. The simulation provides a good approximation about the bed hydrodynamics and formation of products. Thus the results can be compared well with the experimental results. Therefore the results can further be implemented to scale up the reactor as per the needs or for optimum design.

1.4 Obective of the work

It is observed that modeling of FBR using a process simulator such as ASPEN PLUS has been limited to simple mass and energy balances with no information available about the bed hydrodynamics. From the literature survey it is found that studies on bed hydrodynamics needs more attention. Therefore the objective of the present work is planned as follows

- To study the fluidization characteristics of different sized solid particles inside the FBR.
- To study the effect of different system parameters on hydrodynamic behaviors of the FBR.
- To analyze the bed materials before and after the reaction.
- To study the bed hydrodynamics inside the Metallic FBR using ASPEN PLUS simulation.
- To validate of bed hydrodynamics and reaction results obtained from experiments and ASPEN PLUS simulation.

1.5 Thesis Layout

The Thesis is comprised of Six Chapters

1st Chapter: The first chapter describes the introduction to the research work.

2nd Chapter: The second chapter gives a comprehensive review of the different fluoride abatement techniques currently used in the industries, selection of bed materials and the details about the bed materials like its properties and uses. Theoretical background on some of the physical characterization techniques such as ICP-MS, PSA, XRD, BET, FTIR and FESEM analysis are described in this chapter as well as the computational aspects by ASPEN PLUS for the hydrodynamics behaviors of gas-solid fluidized bed are also studied in this chapter.

3rd Chapter: The third chapter highlights the experimental setup, materials and methods used for the abatement of Fluorides from the industrial effluent. This chapter also describes the details about the Fluidized Bed Reactor which was set up in the laboratory and its various components.

4th Chapter: The fourth chapter deals with the Hydrodynamic studies obtained using ASPEN PLUS Simulation. The various results obtained from the simulation have also been discussed thoroughly in this chapter.

5th Chapter: The fifth chapter describes the results obtained after the reaction. This chapter also compares both the experimental and simulated results.

6th Chapter: The sixth chapter deals with the conclusions that have been drawn on present work and scope of the future work.

CHAPTER – 2

LITERATURE SURVEY

Fluorine is widely dispersed in nature and is estimated to be the 13th most abundant element on our planet [1]. The time-weighted average exposure limit for an 8-hour day or a 40-hour week is 1 ppm. So the fluoride coming out from process industries needs to be treated before venting it to the atmosphere. Many methods have been developed by the researchers for the treatment of gaseous effluents containing fluorides. No methods is so far found to be very efficient one for which research is still going on to develop a better method so that the fluoride levels in the atmosphere can be minimized.

2.1 Different methods available for abatement of fluoride:

Different methods are used by the researchers for abatement of fluorides. Brief description for these methods is given below.

2.1.1 Dilution Treatment: In this method, non-reactive gases are added in the effluents gas stream to lower the concentration of fluorides and other hazardous materials. At high concentrations, fluoride reacts exothermically with all elements except oxygen, nitrogen and noble gases. Therefore this method is considered to be a reasonable alternative for the abatement of fluorides with naturally occurring reactions without adding energy to the system [2].

2.1.2 Dry Abatement: In this method, the fluoride gas stream is allowed to flow through a dry bed filled with a reactive material. Activated Alumina is generally used as a bed material to treat the gas in counter flow manner. This system requires large flow cross-

section for which this method is not economically unviable [2]. Again this method requires large quantity of activated alumina. Activated alumina is not available as such as its production method involves additional cost and time.

2.1.3 Thermal Abatement: Thermal abatement approach combines reactive materials and fluorides inside a reactor where heat is supplied externally using fuel or electrical energy. Existing thermal unit requires the addition of hydrogen source/fuels such as methane or hydrogen to drive the fluoride reaction to completion thereby converting fluoride into hydrogen fluoride (HF). Further, the generation of by-products by the thermal abatement of fluorides requires the use of a post-treatment water scrubbing process. The removal efficiencies in these scrubbers are often compromised due to the fact that the scrubbing efficiency of most acid gases decreases as the temperature increases. In addition to this, containment of hot concentrated acids requires expensive materials of construction in order to prevent temperature-enhanced corrosive attack on linings, vessels and fittings [3].

2.1.4 Conventional Treatment: This type of treatment involves combustion of the fluoride gas stream with a fuel gas (e.g., natural gas or butane) at temperatures of about 700-800^{0}C in a burn box resulting in the formation of primarily hydrogen fluoride (HF), carbon dioxide (CO_2) and water. In addition to the high heat requirements and the need for a fuel gas, the conventional treatment method suffers from corrosion problems which is majorly due to the formation hydrogen fluoride (HF) [4].

2.1.5 Wet Abatement: In this method, fluorine is reacted with water and the products formed due to the reaction between water (H_2O) and fluoride (F^-) thereby forming hydrogen fluoride (HF), oxygen gas (O_2) and hydrogen peroxide (H_2O_2) [5]. The difficulties associated with this method are the formation of unwanted oxygen di-fluoride (OF_2) and the large water consumption necessary to achieve acceptable removal efficiency at high fluoride concentration.

2.1.6 Point-Of-Use Method: This method is used for plasma abatement of per fluorocarbon compounds (PFC) in semiconductor industries [6]. Point-of-use abatement involves placing a high-density plasma source in the fore line of a process tool between the turbo molecular and dry pumps. Both Vartanian and the SEMATECH disclosure have mentioned that hydrogen gas (H_2) could be an additive gas in the plasma.

2.1.7 Adsorption method: In this process dry adsorbents such as limestone, calcium carbonate, slaked lime, quick lime, alumina, activated alumina and magnesia, are introduced into a conduit traversed by the gas stream which leads to a bag filter in which the particles accumulate in a layer which is traversed by the gas. The particles are allowed to remain in contact with the gas for a brief period of time in the conduit and then these are contacted after they form a layer upon the filter surface. The adsorbent is usually fine-grained and has a mesh size generally smaller than 200 mesh. One difficulty with this system is that segregation of the particles tends to occur and the layer on the vertical pockets of the filter tends to have streaks and regions of different effective thickness and thus a homogeneous contact of the gases with the dust is not ensured. The

contact time between the gas and the particles also tends to be relatively short by which an optimum mass transfer of the HF is not always ensured [7].

2.1.8 Fluidized Bed Method: In this method Fluoride present in the gaseous effluents are reduced by contacting the gas with a bed of suitable materials wherein fluorides are allowed to react with metal particles present in the bed. The process can be conducted in parallel units connected by switching fluidized beds wherein the beds are switched based upon achievement of a predetermined bed expansion. The process can also be conducted in continuous operation where more reduction of fluorides is possible. Thus the gaseous fluorides are converted into solid fluorides such as FeF_2, FeF_3, AlF_3 etc. Metals present in the bed are not greater than 300 microns in size [8].

Thus among the different methods used for the abatement of gaseous fluorides, fluidized bed method is found to be more effective because of better fluid solid contact and also due to the various other advantages associated with the fluidization principle. In this method metal particles are required to be used in the bed.

Gas–solid fluidized beds have been widely used in both the chemical reactions and the physical processes for their excellent gas–solid contacting and relatively uniform temperature/ concentration profiles within the beds. Gas–solid circulating fluidized beds [9, 10] find wide application in the chemical and process industries, such as fluidized catalytic cracking (FCC) [11], combustion [12], alumina calcining [13], and synthesis of fine chemicals like maleic anhydride [14]. More recently, liquid–solid circulating

fluidized beds are also finding applications in the process industries such as in the synthesis of aromatic and olefinic alkylates [15, 16].

2.2 Red mud as Bed Material

Red mud is the solid waste obtained from the digestion of bauxite ores with caustic soda for alumina (Al_2O_3) production. Approximately 35–40% of the processed bauxite ore goes into the waste as alkaline red mud slurry which consists of 15–40% solids and 0.8–1.5 tons of red mud is generated per ton of alumina produced. Its proper disposal is one of the most difficult tasks [17, 18]. That is why over the years, extensive work is being done by researchers worldwide to develop various economic ways for the utilization of red mud. In the current work RM is used as a bed material inside a FBR to abate gaseous fluorides.

2.3 Utilization of red mud

The various RM utilizations that have been investigated includes: (i) as a stabilization material for the preparation of liners [19] (ii) as adsorbents for the removal of heavy metals, dyes, phosphate, nitrate and fluoride [20] (iii) preparation of catalysts [21] (iv) recovery of iron, aluminium, titanium and other trace metals [22] (v) production of radiopaque materials [23] (vi) preparation of ceramics [24, 25] (vii) production of construction bricks [26] (viii) development of pigments and paints [27] and (ix) preparation of cements [28-30]. Considerable research and development work for the storage, disposal and utilization of red mud is being carried out all over the world [31-

35]. It gives the detailed appraisal of the work being carried out for making use of red mud in building, pollution control and metal recovery.

The chemical composition of red mud contains six major constituents, Chemical analysis shows that red mud contains silicon, aluminium, iron, calcium, titanium, sodium as well as an array of minor elements namely K, Cr, V, Ba, Cu, Mn, Pb, Zn, P, F, S, As and etc. The variation in chemical composition between red mud obtained from various places throughout the world is high. Typical composition of red mud is given in Table 2(a) [36]. Typical chemical composition of red mud generated by Indian alumina plants is as given in Table 2(b) [37]. The major chemical composition of red mud for selected countries over the world is presented in Table 2(c). These data indicate that Al_2O_3 and Fe_2O_3 are major components of RM and many other metals are also present in traces. In addition to that RM is plentily available at free of cost being the waste material

Generally, the major mineralogical phases of red mud from the Bayer process are gibbsite ($Al(OH)_3$), boehmite (γ-AlOOH), hematite (Fe_2O_3), goethite (FeO(OH)), quartz (SiO_2), rutile (TiO_2) and calcite ($CaCO_3$), and the principal mineralogical constituents of red mud from the sintering process are β-$2CaO.SiO_2$, calcite ($CaCO_3$), hematite (Fe_2O_3), gibbsite ($Al(OH)_3$) and perovskite ($CaTiO_3$).

The key to solving red mud stockpiling which is practised in the aluminium industries is to develop a comprehensive utilization technology that consumes red mud or converts it into a secondary resource. Over the years scientists have carried out various research projects that explore disposal and utilization of red mud according to the unique physical and chemical properties of red mud. Some of them are discussed as follows.

2.3.1 Recovery of Red Mud Components

Red mud primarily contains elemental components such as, Fe_2O_3, Al_2O_3, SiO_2, CaO, Na_2O and K_2O. Besides, it also contains other components, such as Li_2O, V_2O_5, TiO2 and ZrO_2. For instance, the content of TiO in red mud produced in India can be as much as 24%. Because of the huge amount of red mud, value elements like Ga, Sc, Nb, Li, V, Rb, Ti and Zr are valuable and abundant secondary resources [38]. Therefore, it is of great significance to recover metals, especially rare earth elements from red mud.

2.3.2 Production of Construction Materials from Red Mud

The bulk production of building materials could eliminate the disposal problem. Bauxite residues have other options for its reuse in preparation of construction materials such as, clay based product [39], glass [40], aerated concrete block [41] etc.

2.3.3 Red Mud used as a filling material

Red Mud can also be used as a filling material for the construction of Road based material [42], backfill material in mining [43] and also providing anti-ageing properties in PVC products [44].

Apart from all those mentioned above Red Mud can also be used in some pollution control activities such as waste water improvement, soil improvement, treatment of waste sulphur containing gases, coagulant, adsorbent and catalyst [45-51].

That is why it is planned to use RM as a bed material so that necessary metal requirements for the reaction with fluorides can be achieved. Before using RM for the abatement of fluorides, it is required to know the characteristics or properties of the available RM.

Thus it is planned to study the fluidization characteristics of the red mud in the present work before using it as a bed material inside in a FBR . Red mud is a very fine grained material. Typical values for particle size distribution are 90 weight % below 82.5 microns. The specific surface area (BET) of red mud is between 10 and 30 m^2/g, depending on the degree of grinding of bauxite. The particle size and density of RM places it under Geldart A category solids [52, 53]. Fluidization quality is closely related to particle intrinsic properties such as particle size, particle density, size distribution of particle and its surface characteristics. As the particle size decreases the cohesive force (i.e. Vander Wall Force) for the particle increases. As a result of this the fluidization of cohesive materials for fine particle becomes much more difficult in comparison to the larger size particles. Geldart A solids exhibits bubbling fluidization.

2.4 Material Characterization Techniques

In order to understand the red mud characteristics when it is fluidized in the reactor above the minimum fluidization velocity various samples are collected at different temperatures i.e. room temperature, 150^0C (423.15K), 200^0C (473.15K), 250^0C (523.15K) and 500^0C (773.15K). The reactor takes a total time of approximately 2.5 hours to reach 500^0C (773.15K). After fluidization the samples are collected and stored inside sealed plastic packets after the samples are cooled to room temperature. The XRD pattern of the

material and the material composition are analyzed using PHILIPS X'Pert X-Ray diffractometer with a Cu Kα radiation source in a 2θ range of 10^0 to 70^0 at spanning range of 3^0 min^{-1}. The conditions are kept same while analyzing the red mud and red mud containing aluminum samples obtained after the reaction. The TGA and DTA analysis technique is carried out using SHIMADZU DTG-60H. In this analysis 17.361 mg ($17.361x10^{-6}$ Kg) of the RM sample at room temperature is used. The sample is heated in an alumina crucible at a heating rate of 10^0C min^{-1} (283.15K min^{-1}) from 28^0C (301.15K) to 500^0C (773.15K) in Nitrogen atmosphere where the gas flow rate is 35 ml min^{-1} (0.035 l min^{-1})The particle size of the samples are measured using MALVERN MASTERSIZER (Hydro 2000MU) . FESEM and Energy Dispersive X-Ray (EDX) are used to study the surface morphology and elemental composition of the samples respectively using NOVA NANO SEM 450.

The FT-IR spectra of the samples are obtained by using Perkin Elmer FT-IR Spectrometer (Spectrum RX-I). The range is taken between 4000-400 cm^{-1}. Each of the samples is mixed with Anhydrous KBr and is then pressed at 10 tons/cm^2 pressure to make translucent tablets required for recording of FT-IR spectra. The BET surface area of the samples is also measured by QUANTACHROME AUTOSORB-1 using liquid N_2.

The Inductively Coupled Plasma Mass Spectrometry or ICP-MS is carried out at NML Jamshedpur to find the elemental composition of the samples. It is an analytical technique used for elemental determinations. This analysis has superior detection capabilities, particularly for the rare-earth elements (REEs). ICP-MS has many advantages over other elemental analysis techniques such as atomic absorption and

optical emission spectrometry. The advantages of using this methods are described as follows.

- Detection limits for most elements equal to or better than those obtained by Graphite Furnace Atomic Absorption Spectroscopy (GFAAS).
- Higher throughput than GFAAS method.
- The ability to handle both simple and complex matrices with a minimum of matrix interferences due to the high-temperature of the ICP source.
- Superior detection capability to ICP-AES with the same sample throughput.
- The ability to obtain isotopic information.

2.5 ASPEN PLUS Simulation:

The traditional approach necessary to establish commercial plant is based on comprehensive experimental investigations and processing from a laboratory scale test unit to a pilot scale plant, before building a full scale commercial demonstration plant. However this does not take in account practical problems associated with large units. Therefore researchers work on modeling and simulation. Various mathematical models as well as simulations are now developed in the recent years for the successful modeling of the FBR's.

Various process simulator programs such as ASPEN PLUS, PRO/II, HYSIS, CHEMCAD, DESIGN II etc. are available and are employed for process simulation purposes by industrial entities. All these programs have been developed based on the sequential modular approach, i.e. they consist of different standard modules which could

be combined together to represent the whole process. These process simulators are generally not strong in reactor modules and only contain standard ideal reactors such as PFR and CSTR. The standard modules have to be combined in a logical way to represent the reality in the FBR's. Furthermore the model has to be easily applicable in all process simulation programs. ASPEN PLUS is large-scale chemical process software which is based on steady chemical process simulation, optimization and sensitivity analysis and economic evaluation. It provides customers a complete set of unit operation model to simulate the process of operation, from a single operation unit to the entire process simulation [54]. Weiss et al. [55] introduced a CFBC model by dividing it into 11 blocks, each corresponding to a CSTR reactor for both gas and solid phases. Five of these blocks are related to the CFBC riser. Basu et al [56] developed a CFBC model in which a plug flow regime for both the gas and solid phase is assumed. Lee and Hypanen [57] presented a CFBC model which considers the riser as a plug flow reactor for the gas phase and a CSTR for the solid phase where the feed particle size distribution and the attrition phenomena are considered. The work of Young [58] entails the modeling and simulation of FBC using ASPEN where a 'black box' approach with one ASPEN PLUS stoichiometric reactor is used to calculate the mass balances based on given combustion and sulfur capture efficiencies. CFBC simulation work was also initiated at CERCHAR [59] to provide the technical information required for the evaluation and optimization of CFBC's under steady-state condition in power generation applications. The approach used at CERCHAR is similar to that of Young, but is extended to cover CFBCs.

All the above mentioned works with the various models and follows a sequential modular approach in order to model the reactors but very little almost no work is

available on the study of the hydrodynamics for the FBR. Therefore it is planned to use ASPEN PLUS V8.4 software where the bed hydrodynamic study is possible only with this version of ASPEN PLUS. The characteristics change in RM composition before and after reaction are also planned to be studied using ASPEN PLUS simulation.

TABLES

Table 2(a). Typical composition of Red Mud

Composition	Weight %
Fe_2O_3	30-60
Al_2O_3	10-20
SiO_2	3-50
Na_2O	2-10
CaO	2-8
TiO_2	25

Table 2(b). Chemical composition of Indian Red Muds

Company	Al_2O_3%	Fe_2O_3%	SiO_2%	TiO_2%	Na_2O%	CaO %	LOI %
BALCO Korba	18-21	35-37	6-7	17-19	5-6	2-3	11-14
HINDALCO Renukoot	17-19	35-36	7-9	14-16	5-6	3-5	10-12
HINDALCO Muri	19-21	44-46	5-7	17-19	3-4	1-2	12-14
HINDALCO Belgaum	17-20	44-47	7-9	8-11	3-5	1-3	10-14
MALCO Metturdam	18-22	40-26	12-16	3-4	4-5	1-3	11-15
NALCO Damonjodi	17-20	48-54	4-6	3-4	3-5	1-2	10-14

Table 2(c). Major chemical composition of red mud generated in alumina plants in various countries

Country	Plant	Major Composition (Wt %)					
		Fe2O3	**Al2O3**	**TiO2**	**SiO2**	**Na2O**	**CaO**
Australia	AWAAK	28.5 2	24.0	3.11	18.8	3.4	5.26
Brazil	Alunorte	45.6	15.1	4.29	15.6	7.5	1.16
Canada	ALCAN	31.60	20.61	6.23	8.89	10.26	1.66
France	Aluminum Pechiney	26.62	15.0	15.76	4.98	1.02	22.21
Germany	AOSG	44.8	16.2	12.33	5.4	4.0	5.22
Italy	Eurallumina	35.2	20	9.2	11.6	7.5	6.7
UK	ALCAN	46.0	20.0	6.0	5.0	8.0	1.0
USA	RMC	35.5	18.4	6.31	8.5	6.1	7.73

CHAPTER –3

EXPERIMENTATION

Preliminary experiments are carried out using a perspex column having the same dimensions inside which the reaction is intended to take place (Fig.3.0). The minimum fluidization velocity obtained at a particular air flow rate is noted and the same flow air rate is taken as the minimum fluidization velocity for the next experiment which is intended to carry out in a high temperature Fluidized Bed Reactor. A stainless steel made Fluidized Bed Reactor has been designed and set up in the laboratory. Red Mud of definite size is selected as the bed material and the various phase changes which occurred inside the high temperature Fluidized Bed is studied. After that two sets of experiments were carried out where the effluent gas containing fluorides obtained from the industries were allowed to mix with the fluidizing gas thereby fluidizing the bed material. In the first case only red mud is used as the bed material whereas in the second case red mud-aluminum mixture is considered as the bed material. The bed materials are fluidized using an air blower.

3.1 Experimental Set-Up

Fig 3.1(a-h) and Fig 3.2 shows the different components of the experimental set-up and the schematic diagram of the experimental setup respectively. An air blower of the following specifications is used to fluidize the bed material. (2850 RPM, 180 Watts and Temperature rise: 3-82.5^{0}C (276.15-355.65 K)). The reactor and the pipes used to build up the FBR is made up of Stainless Steel 316 grade and is fabricated with the help of Mechmomine Kolkata and is able to withstand pressures till 5 atm (506625 Pa) . The

length of the reactor column in 20.5" (0.5207m) and the internal diameter is 4" (0.1016m) with 0.39" (0.009906 m) thickness. The reactor is bounded in both the sides with cones of 4" (0.1016m) height and 4" (0.1016m) internal diameter, the thickness being same as the reactor column. The removable bolt joint between the cones and the reactor column is provided with iron heat gaskets to prevent leakage. A ceramic heater is connected to the periphery of the FBR which is capable of heating the FBR to a maximum temperature of 500^0C (773.15 K) and a tubular heater is provided just after the air blower in the setup assembly which is 12" (0.3048 m) in length, having 1.5" (0.0381m) internal diameter and 0.2" (0.00508m) thickness. The heater uses 0.047" (0.0011938m) Nichrome wire to heat the heater tube. This heater acts as an air heater which is capable to heat air to a maximum temperature of 100^0C (373.15 K). The bases of the cones are provided with wired meshes of size approximately 40 microns ($40x10^{-6}$m). This wired mesh acts as the gas distributor in order to fluidize the bed materials. The reactor is also provided with two gate valves and one globe valve. The globe valve is used to maintain the air flow rate from the air blower. The gate valves are used to either allow the gas to circulate or stop it at certain points.

3.2 Materials and method:

3.2.1 Characterization of bed materials

The Red Mud used in this study is collected from NALCO, Damanjodi, Odisha, India and the aluminum is purchased from local stores. The Effluent Gas containing Fluorides is obtained from an Aluminum Industry.

Air is used as the primary fluidizing medium for the experiment where industrial Effluent Gas obtained from the Aluminum Industries (E.Gas) is used as the secondary gas. The air flow is maintained using a blower. The typical gas composition obtained from the exhaust of the Aluminum Industry [60] is shown in Table 3(a).

Red Mud sample as collected is analyzed for knowing about different components present in it. After experiments the bed materials are also analyzed. The various elements present in the bed materials before and after the experiments are compared. The comparison among the results for these cases indicates that reactions have taken place for which composition have changed. ICP-MS analysis report is shown in Table 3(b).

The bed material is of great importance for a fluidized bed reactor without which Fluidized Bed Reactor (FBR) cannot be designed. Bed material acts as one of the reactants. In some cases bed material may also act as a catalyst. Red Mud (RM) powder with an average particle size of 77 microns ($77x10^{-6}$m) is used for this application. The small particle size provides adequate fluidization for the RM bed and more surface area for reaction between the metallic oxides present in RM with Fluorine species. In the second experiment the bed is considered to be a mixture of 77 microns ($77x10^{-6}$m) RM and 82.5 microns ($82.5x10^{-6}$m) Aluminum in the ratio 9:1. These sizes of RM and Aluminum particles are considered as some preliminary studies suggested that they have better fluidization quality.

3.2.2 Material Preparation

The RM is produced in slurry form. On drying this slurry, lumps of RM are produced. The collected RM lumps are initially ground inside a ball mill and are then sieved. The

red mud particles are ground to sizes 103 ($103x10^{-6}$m), 90 ($90x10^{-6}$m), 77 ($77x10^{-6}$m) and 53 microns ($53x10^{-6}$m) by sieve analysis technique. The aluminum particles are also ball milled to obtain fine aluminum particles of 82.5 microns ($82.5x10^{-6}$m) size. The RM particles of 77 microns ($77x10^{-6}$m) size is found to have better fluidization quality and is thus considered for the experiment.

3.2.3 Methods:

Preliminary experiments were carried out inside a perspex column (Fig 3.0) to understand the bed behavior when the bed was allowed to fluidize with atmospheric air. Depending on the observations from the perspex column experiments, same amount of RM is then fed into the Stainless steel column to study the effect of temperatures on the phase transition of red mud when it was allowed to fluidize above minimum fluidization velocity. Various characterizations were also carried out in support to it. Depending on the results obtained, two more experiments were carried out where Effluent Gas obtained from the industries was used as a secondary gas.

In the first experiment 1000 grams (1Kg) of Red Mud ($77x10^{-6}$m) was fluidized with a mixture of air and the effluent gas. The air was supplied by the blower and the Effluent Gas was supplied from the stainless steel made sampling cylinder. The bed was allowed to run at a temperature of 250°C (523.15 K) and a residence time of 30 minutes was given where the effluent gas mixes with the bed materials. The bed material samples were then collected.

In the second experiment 900 grams red mud ($77x10^{-6}$m) and 100 grams (0.1 Kg) ($82.5\ x10^{-6}$m microns) aluminum powder was used as a bed material which was then

fluidized with the mixture of air and effluent gas at 250^0C (523.15 K). This step is done in order to provide better fluidization because similar sized particles of very small sizes may sometimes get agglomerated leading to improper fluidization. So in order to prevent this, aluminum powder of slightly bigger size is preferred so that proper fluidization can be achieved and also the reaction characteristics of the Effluent Gas with the red mud and aluminum powder can be checked. The bed materials before and after are then compared.

Before the experiments were carried out the effluent gas was collected from an Aluminum Industry and was stored in a 5 L capacity cylinder having needle valves at both the sides. One of the opening of the gas cylinder was connected to the lower cone of the stainless steel made fluidized bed reactor via an air rotameter by the help of which we can control the Effluent Gas flow rate which then mixes with the air coming from the air blower so that the combined velocity becomes more than the minimum fluidization velocity and less than the entrainment velocity (the velocity at which the be materials comes out of the reactor) thereby having proper fluidization.

3.2.4 Simulation Data:

Depending upon the previous discussions about the methods used the simulation is carried out. The data used for ASPEN PLUS Simulation are shown in Table 3(c).

TABLES

Table 3(a). Typical composition of Effluent Gas obtained from Al-industry

Components	Percentages (%)
HF	20
O_2	30
NO	10
CO	10
CO_2	20
SO_2	10

Table 3(b). Composition of bed materials before and after the experiment.

Elements %	Bed Material before experiment (Red Mud)	Bed material after Experiment 1. (Red Mud + E.Gas)	Bed material after Experiment 2 (Red Mud + Al + E.Gas)
SiO_2	4.96	5.54	8.12
Al_2O_3	13.72	16.19	37.41
Fe_2O_3	50.29	55.24	40.51
TiO_2	5.08	5.83	4.31
Na_2O	4.62	3.94	2.73

Table 3(c).Various parameters used in the simulation

Parameters	Experiment 1	Experiment 2
Property Method	WILS-HF	WILS-HF
Bed Mass	1 Kg	1 Kg
Bed Material	Red Mud	Red Mud + Al (9:1)
Voidage at minimum fluidization	0.5	0.5
Minimum Fluidization velocity	0.014 m/s	0.027 m/s
Transport Disengagement Height (TDH) model	George & Grace	George & Grace
Elutriation model	Tasarin & Geldart	Tasarin & Geldart
Height of Column	20 inches (0.508 m)	20 inches (0.508 m)
Diameter of column	4 inches (0.1016 m)	4 inches (0.1016 m)
Gas Distributor Type	Perforated Type	Perforated Type
Number of orifices	2310	2310
Orifice Diameter	40 microns($40x10^{-6}$m)	40 microns($40x10^{-6}$m)
Operating Pressure	1 atm (101325 Pa)	1 atm (101325 Pa)

FIGURES

(a) RM at static condition

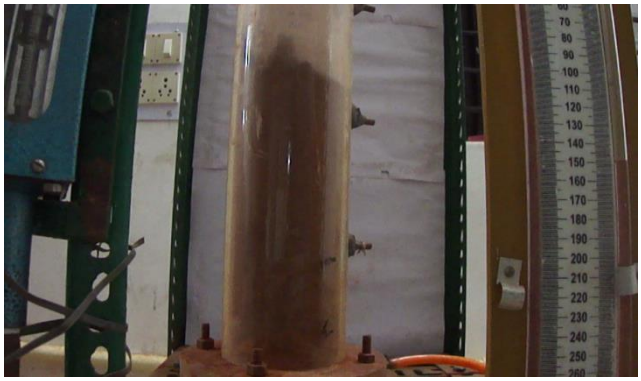

(b) RM at fluidized condition

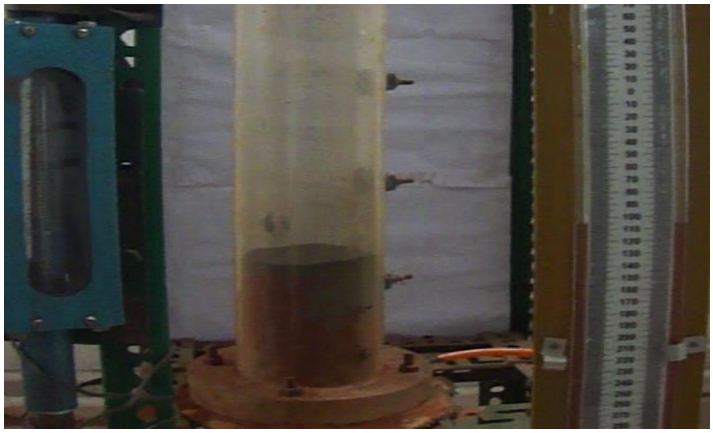

(c) RM-Al mixture at static condition

(d) RM-Al mixture at fluidized condition

Fig.3.0 Pictures of fluidized bed for different bed materials

(a) Front View of the Reactor Column

(b) Top View of the Reactor Column

(c) Top view of the cone

(d) Front view of the cone

(e) Front view of the Tubular Heater

(f) PID Controller

(g) Blower

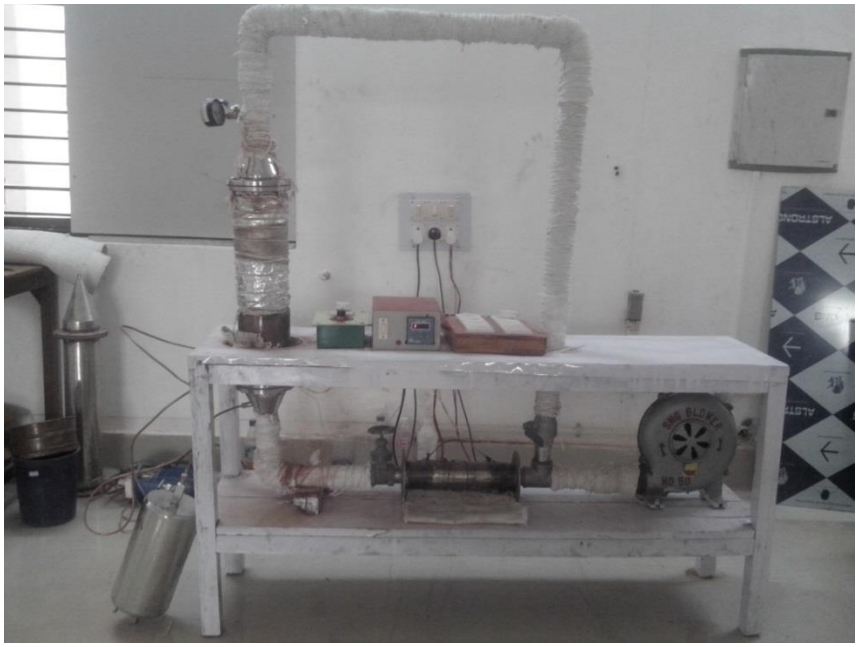

(h) Actual experimental setup of the Fluidized Bed Reactor

Fig 3.1(a-h) Pictures of different parts of the experimental setup

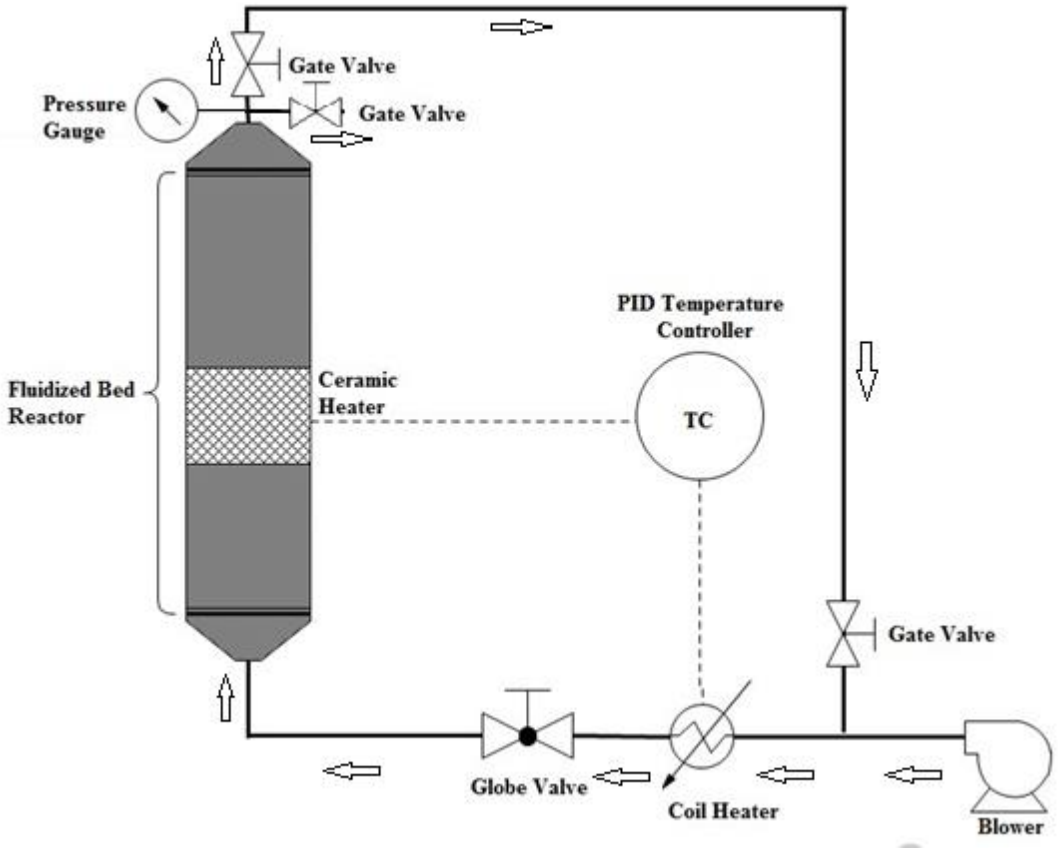

Fig 3.2 Schematic diagram of the experimental setup

CHAPTER – 4

ANALYSIS OF BED HYDRODYNAMICS USING ASPEN PLUS SIMULATION

4.1 INTRODUCTION

Fluidized Bed Reactor is designed to be used for the abatement of Fluorides. For proper design of FBR it is essential to have knowledge on hydrodynamics of fluidized bed. Again it is impossible to carry out experiments directly without knowing anything on operation of a fluidized bed. That is why it is thought of carrying out simulation first for the hydrodynamics of a fluidized bed so that the effect of input parameters can be studied thoroughly. ASPEN PLUS Simulation is selected for the present work.

ASPEN Plus is a steady state chemical process simulator which uses unit operation blocks. These are models of specific process operations (reactors, heaters, pumps etc.). These blocks are placed on a flow sheet which represents the material and energy streams. An extensively built in database of physical properties is used for the simulation calculations. The development of a model in ASPEN Plus involves the following steps:

- Specification of stream class and selection of property method.
- Specification of system component (From databank).
- Defining the process flow sheet (unit operation blocks and connecting material & energy streams).
- Specification of feed streams (flow-rate, composition and thermodynamic condition).
- Specification of unit operation blocks (thermodynamic condition, chemical reactions etc.).
- The hydrodynamic studies for the fluidized bed reactor are carried out using ASPEN PLUS Simulation. The simulation package determines the various aspects of fluidization

process such as the minimum fluidization velocity, height of the bottom zone, height of freeboard, TDH, solids holdup, distributor pressure drop, bottom zone pressure drop, freeboard pressure drop, fluidized bed pressure drop as well as the reaction products and bi-products. Apart from this various graphs such as PSD curve, superficial velocity curve, interstitial velocity curve, solids volume fraction curve, pressure curve, bubble volume fraction curve, bubble rise velocity curve and bubble diameter curve can also be obtained from the ASPEN PLUS Simulation package.

4.2 Flow Sheet development:

The FBR can be modeled using Aspen Plus user interface. Both the reaction products and bed hydrodynamics can be obtained from this simulation. The Aspen Plus model of the FBR has been shown in Fig 4.1(a-b).

From the Fig 4.1(a) it is seen that the stream named "RM-IN" represents the RM inlet where RM is used as a feed and in turn as the bed material. Fig 4.1(b) shows stream "AL-IN" indicating Aluminum (Al) is used as the additional bed material. Air is supplied using an air blower. The Effluent Gas obtained from the Aluminum Industry (E.Gas) is passed through the FBR for treatment of Fluorides. The effluent gas is allowed to mix with the air coming from the blower just before the air distributor plate of the FBR. Part of the outlet stream coming out from the GIBBS Reactor named as "RECYCLE" is recycled back to the FBR in order to keep the mass flow rate of RM constant so that the bed mass remains constant throughout the operation. The "GIBBS-OUT" stream indicates the output stream coming out from the GIBBS Reactor. The air supplied by the blower is passed to the FBR via a heater which is used to pre-heat the fluidizing air.

4.3 Assumptions:

Certain assumptions are considered while designing the FBR

- Gas in plug flow.
- Solids ideally mixed.
- Each cell is considered as CSTR.
- Isothermal Fluidized Bed.

4.4. Results and Discussion:

4.4.1. Model Validation:

In order to validate the simulation results, the ICP-MS analysis report is used for the validation. The change in the mineralogical composition of RM and RM + Al after the reaction is compared in Table 4(a). The necessary temperature for the abatement of Fluoride as observed in a separate similar simulation [61] where the temperature of 250^0C (523.15 K) is found out to be most suitable for the maximum Fluoride abatement. Minor differences in the RM composition are observed from the simulation results. This is may be due the assumptions of steady state and isothermal condition.

4.4.2. Bed Hydrodynamics:

Table 4(b) compares the change in the bed parameters according the experiment and the simulation. With the increase in temperature various hydrodynamic changes are observed inside the column containing RM in the first case and RM-Al mixture in the second case. The different changes observed are described under the following sub-headings.

4.4.2.1 Particle Size Distribution (PSD):

Red mud sample is analyzed in a Particle Size Analyzer. The mass fractions of the different sized particles are obtained. The values thus obtained are directly used to obtain the PSD curve for the simulation. Fig 4.2 (a, b) and Fig 4.3 (a, b) shows the mass fraction and cumulative mass fraction PSD curves for the RM and RM-AL mixture respectively. From these PSD curves it is observed that most of the particles are smaller than 50 microns in size, i.e. very less particles are above 50 microns size.

4.4.2.2 Interstitial Velocity:

The interstitial velocity is defined as the velocity of gas within the voids or spaces between particles. Interstitial velocity is determined from simulations and expressed as function of fluidized bed height. Thus the obtained simulation results are plotted against the height of fluidized bed as shown in Fig.4.4 (a, b). Interstitial velocity along the height generally increases; this is connected with the free area that is available at any cross section. From the figure it is seen that the interstitial velocity increases with bed height up to a certain level and then it decreases. This may be due to the reason that the amount of void spaces increases with air flow rate. After sometime when the bubbles break or the bubble terminal velocity exceeds the fluidization velocity, the bed height decreases thereby reducing the void spaces. Thus the interstitial velocity decreases. It is also observed that with the increase in temperature the value of the interstitial velocity increases. This may be due to the fact that with increased temperature the bed material becomes more free flowing. As a result they expand to a higher extent with increasing air

flow rate. Thus the void spaces increases with the increase in temperature thereby creating environment for increasing interstitial velocity.

4.4.2.3 Superficial Velocity:

From Fig 4.5 (a, b) it is observed that bed height increases with superficial gas velocity. It is also observed that the amount of superficial velocity increases with the increase in temperature, the main reason is probably due to the increase in volume of gases (from gas law). Since the cross sectional area is the same, superficial velocity increases with the increase in temperature.

4.4.2.4 Pressure Curve:

The bed pressure drop measured at different bed heights are shown in Fig. 4.6 (a, b). It is seen that the bed pressure drop is maximum in the lower part of the reactor and then it decreases with height. The decrease in pressure is due to the transformation of bed from packed to fluidized condition.

4.4.2.5 Solids Volume Fraction Curve:

The solids volume fraction observed from simulations are plotted against the bed height in Fig.4.7 (a, b). From this figure it is observed that solid volume fraction increases with bed height up to certain limit and then decreases. The reason may be due to the fact that when air is allowed to flow through the static bed, the bed material just above the distributor vibrate and try to move upward with the continuous supply of gas from the bottom. Solid bed materials at the bottom layer pushes upward. As a result all the void spaces are filled up within the bed without changing the top layer. Thus solids volume fraction increases with bed height till the minimum fluidization after which void fraction

increases with the increase in gas velocity. Thus solids volume fraction decreases with the increase in bed height. No significant change in the solids volume fraction is observed when the temperature was increased till 250°C (523.15 K).

4.4.2.6 Bubble Diameter:

The bubble diameter as noted from the simulation is plotted against the bed height (Fig.4.8 (a, b)). It is seen from the figure that bubble diameter increases with bed height. The reason may be frequent bubble formation with the increased gas velocity followed by rapid bubble coalescence. As a result the bubble size is found to increase with the bed height. When the terminal velocity of the solid particles exceeds the fluidization velocity only the gas remains in the upper part of the reactor.

4.4.2.7 Bubble Rise velocity Curve:

Bubble velocity obtained from the simulation is plotted against the bed height in Fig.4.9 (a, b). As explained in the bubble diameter section, the bubble size increases with the bed height. With the temperature effect more vigorous fluidization takes place thereby increasing the bubble rise velocity. Thus bubble rise velocity increases with bed height and increased temperature. At lower temperature and lower heights, these plots show discontinuous lines. This may be due to the breakage of bubbles.

4.4.2.8 Bubble Volume Fraction Curve:

Bubble volume fractions against the bed height are shown in Fig.4.10 (a, b). From the figure it can be seen that with the increase in bed height the bubble volume fraction is found to decrease in these plots. This may be due to the fact that in the lower section of the bed more number of smaller bubbles coalesces to form large bubbles which break due

to several factors. Thus it is seen that bubble volume fraction is maximum at the bottom of the bed and minimum in the upper section of the bed.

`Results for both the cases are compared with each other. From Table 4(b) it can be observed that the Fluoride level decreases by 10.0 % when RM is allowed to react with HF at 250°C (523.15 K) whereas Fluoride content decreases by 24.58 % when the material of RM-Al mixture is allowed to react with the E.Gas at that same temperature . The increase in the abated Fluoride content in the second case is because of the fact that HF is more reactive to aluminum than to the other contents present in RM. The decrease in the amounts of Fe_2O_3, Al_2O_3, Na_2O is due to the fact that these oxides react with the Fluoride component present in the E.Gas thereby forming AlF_3, FeF_3 and NaF. The formation of these components is the main cause of the Fluoride abatement. TiO_2 component remains unchanged in its composition as it is known to behave as an inert. Apart from that the amount of SiO_2 is observed to increase which is due to the decomposition of components such as Ca_2SiO_4 and $NaAlSiO_4$ forming extra amount of SiO_2. From Table 4(b) it can also be observed that the amount of NO and CO are almost zero due to the formation of N_2 and CO_2. Significant increase in the amount of H_2O is also observed which is mainly due to the decomposition of Gibbsite. No change is observed in the composition of SO_2. The decrease in the amount of various components is compared against the experimental results. The comparison shows a good approximation about the probable reaction occurring inside the FBR which leads to the successful abatement of Fluorides.

TABLES

Table 4(a) Reaction results obtained from the simulation

Components	RM + E. Gas at 250°C			RM + Al + E.Gas at 250°C		
	Initial (kg/hr)	Final (kg/hr)	Increase ↑ or Decrease ↓	Initial (kg/hr)	Final (kg/hr)	Increase ↑ or Decrease ↓
Fluoride	29.37	26.43	**10.0 % ↓**	29.37	22.15	**24.58 % ↓**
Al	-	-	-	0.464	0.009	**80.6 %**
Fe_2O_3	1.666	1.499	**10.02 % ↓**	1.358	1.222	**10% ↓**
Al_2O_3	0.454	0.409	**9.91 % ↓**	0.371	0.774	**41.48% ↑**
SiO_2	0.164	0.182	**9.89 % ↑**	0.224	0.344	**35.0 % ↑**
TiO_2	0.168	0.168		0.137	0.137	-
Na_2O	0.153	0.132	**13.73 % ↓**	0.125	0.0107	**14.4 % ↓**
FeF_3		0.235		-	0.192	-
AlF_3		0.398		-	1.768	-
NaF			**0.03**	-	0.024	-
O_2	27.961	28.173	**0.82.5 % ↓**	27.961	27.761	**0.7 % ↓**
NO	8.74	Trace		8.74	Trace	-
CO	8.159	Trace	-	8.159	Trace	-
CO_2	25.778	38.477	**33.3 % ↑**	25.778	38.468	**33.3 % ↑**
SO_2	21.318	21.318		21.318	21.318	-
N_2		4.561		-	4.561	-
H_2O	0.003	0.29	**98.9 %↑**	0.003	0.71	**99.5 %↑**
$Al_2O_3.3H_2O$	0.331	0.033	**98 % ↓**	0.27	0.027	**90**
Ca_2SiO_4	0.05	0	**100 % ↓**	0.041	0	**100 % ↓**
$NaAlSiO_4$	0.003	0.002	**33.3 % ↓**	0.003	0.001	**66.6 % ↓**

Table4 (b) Changes in bed parameters under different conditions

	Experimental observed value for RM	Value obtained from simulation for RM at Room Temp.	Value obtained from simulation for RM at 250^{0}C	Experimental observed value for RM + Al	Value obtained from simulation for RM + AL at Room Temp.	Value obtained from simulation for RM + Al at 250^{0}C
Height of bottom zone/ Bed Height	3.5 inches (0.089 m)	3.6 inches (0.092 m)	15.3 inches (0.390 m)	5.5inches (0.145 m)	5.9 inches (0.151 m)	19.9 inches (0.512 m)
Height of Freeboard	16.5 inches (0.419 m)	16.3 inches (0.414 m)	4.658 inches (0.118 m)	14.5 inches (0.368 m)	14.05 inches (0.356 m)	0.1 inches (0.003 m)
TDH	-	16.3 inches (0.416 m)	72.0 inches (1.828 m)	-	14.1 inches (0.356 m)	72.8 inches (1.849 m)
Distributor Pressure Drop		0.00203306 atm (205.99 Pa)	0.00203306 atm (205.99 Pa)	-	0.00213505 atm (216.33 Pa)	0.00213505 atm (216.33 Pa)
Bottom Zone Pressure Drop	-	0.00255669 atm (259.05 Pa)	0.00903878 atm (915.85 Pa)	-	0.0042181 atm (427.39 Pa)	0.0110429 atm (1118.92 Pa)
Freeboard Pressure Drop	-	0.009944188 atm (1007.59 Pa)	0.00293296 atm (297.18 Pa)	-	0.00994811 atm (1007.99 Pa)	0.00294010 atm (297.19 Pa)
Fluidized Bed Pressure Drop	-	0.0119986 atm (1215.75 Pa)	0.0119717 atm (1213.03 Pa)	-	0.0119999 atm (1215.88 Pa)	0.0119829 atm (1114.17 Pa)
Overall Pressure Drop	-	0.0140316 atm (1421.75 Pa)	0.0140048 atm (1419.03 Pa)	-	0.0140310 atm (1421.69 Pa)	0.013082.59 atm (1325.59 Pa)

FIGURES

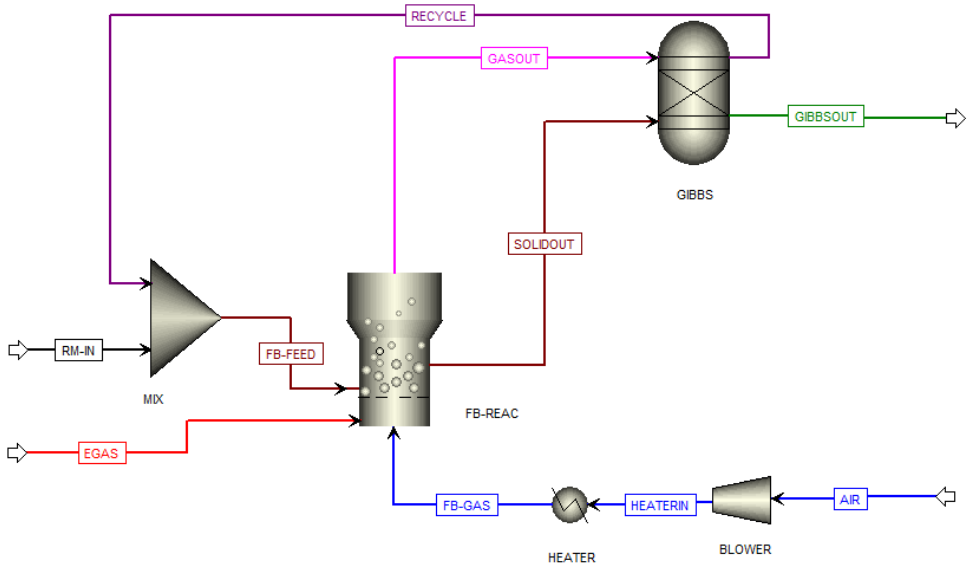

(a): RM as bed material

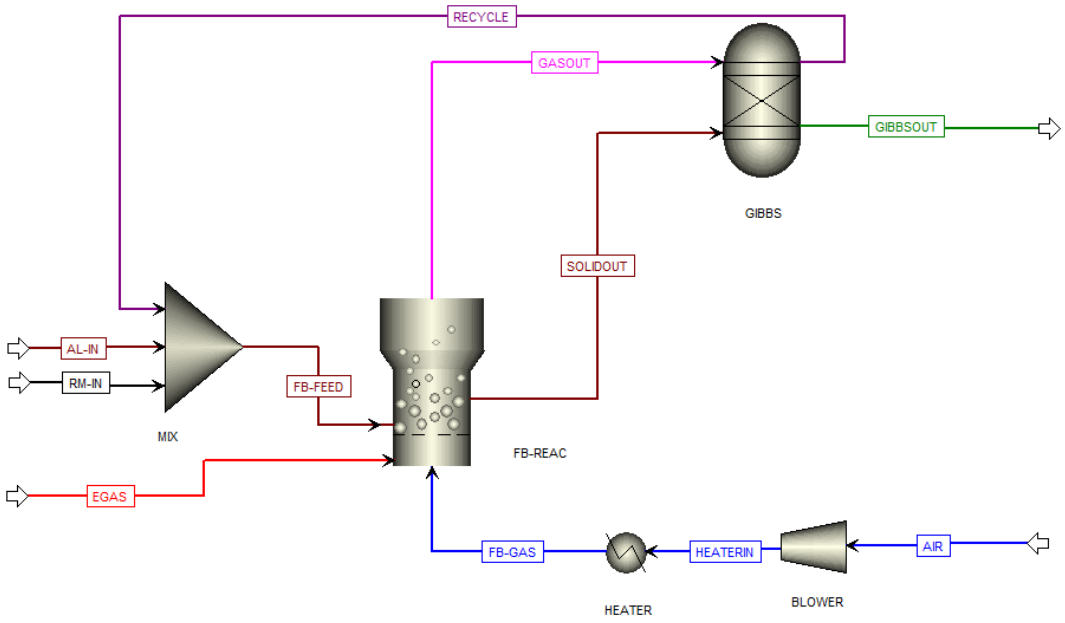

(b): RM –Al mixture as bed material

Fig 4.1(a-b) ASPEN PLUS model of the FBR having different bed materials

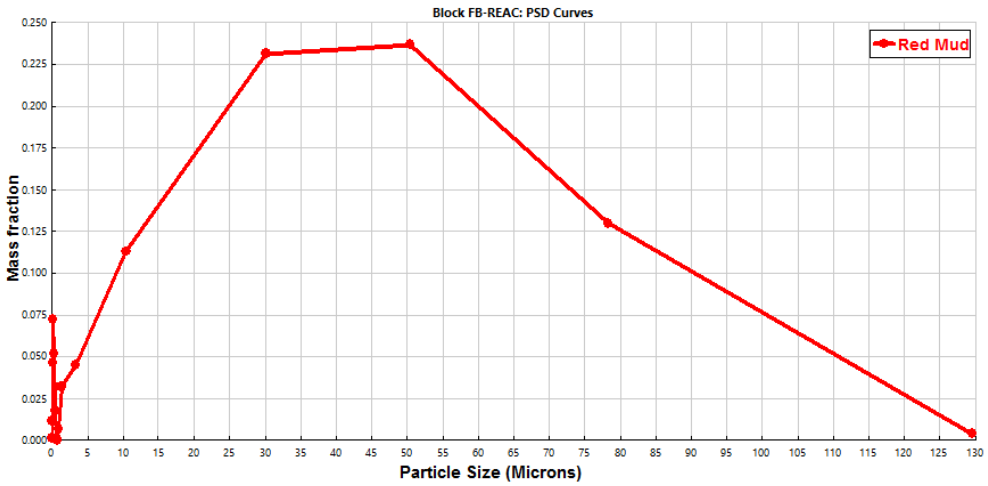

Scale:
X- Axis:
1 Micron =1x10^{-6} m

(a): RM particles

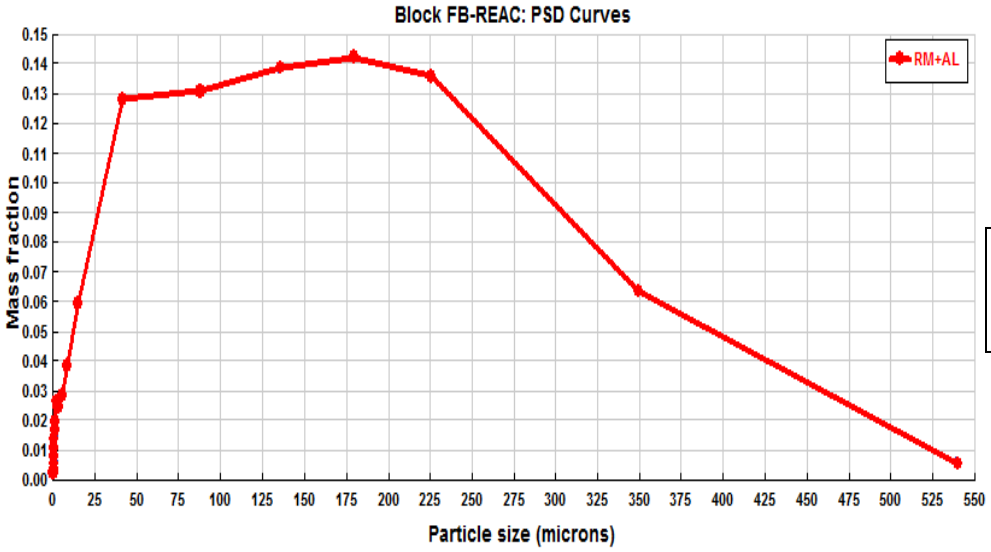

Scale:
X- Axis:
1 Micron =1x10^{-6} m

(b): RM - Al particles

Fig 4.2(a-b) Mass Fraction PSD curves for different bed materials

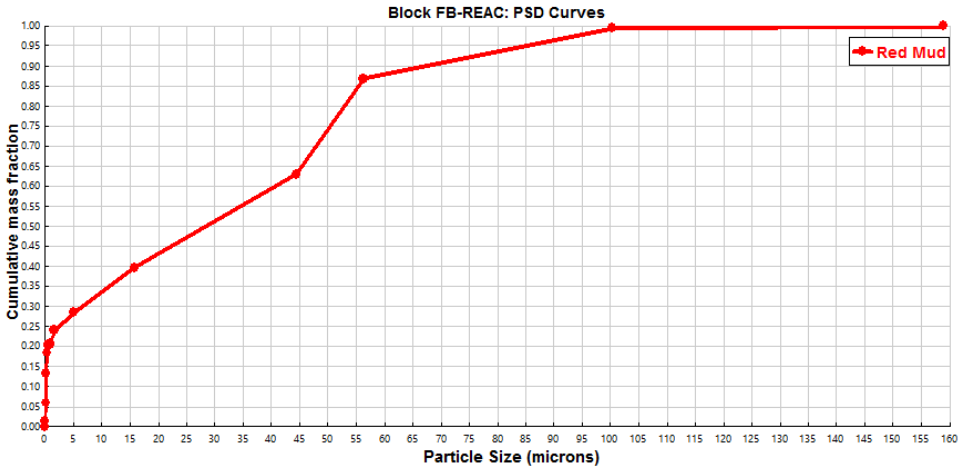

Scale:
X- Axis:
1 Micron =1x10^{-6} m

(a): RM particles

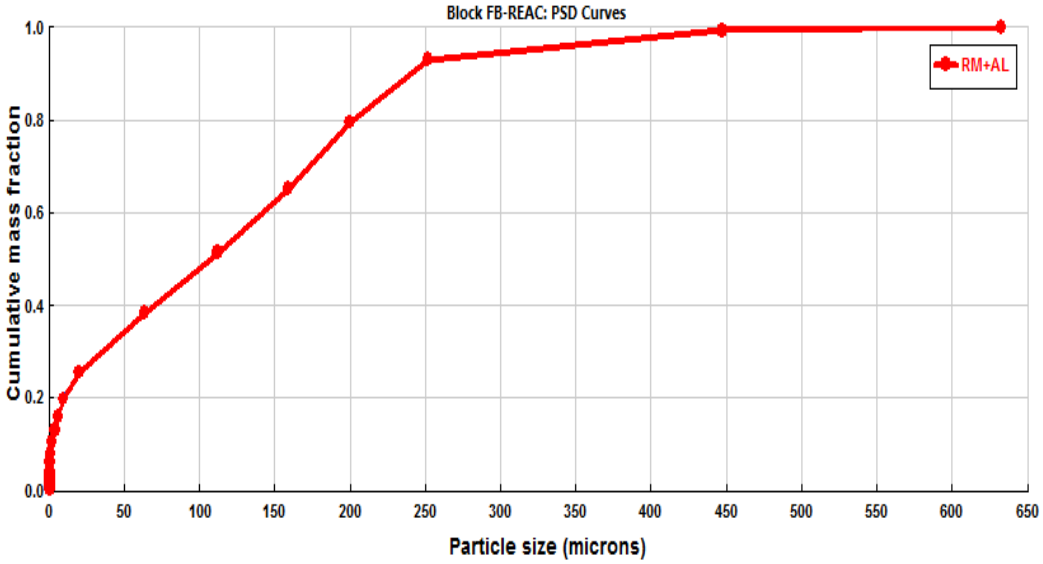

Scale:
X- Axis:
1 Micron =1x10^{-6} m

Fig.4.4 (b): RM -Al particles

Fig 4.3(a-b) Cumulative Mass Fraction PSD curves for different bed materials

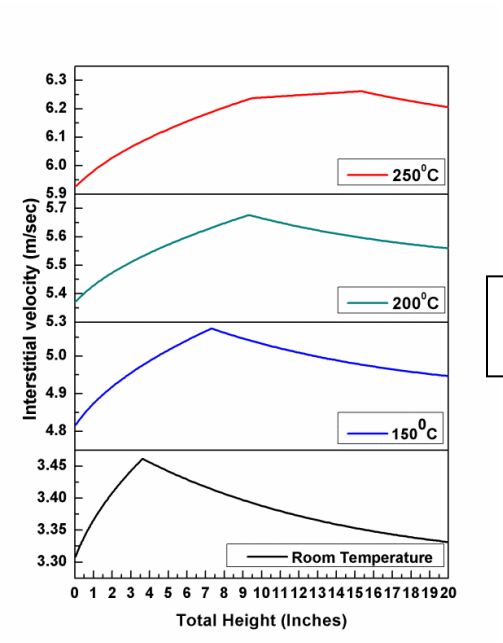

Scale:
X- Axis: 1 inch= 0.0254 m

(a): Bed containing RM

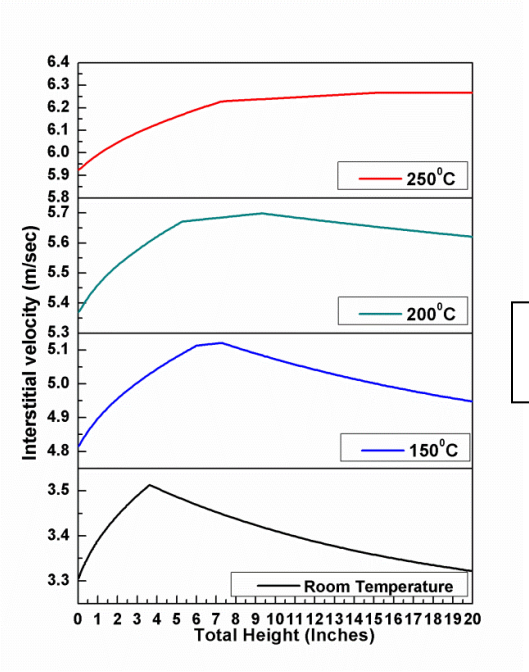

Scale:
X- Axis: 1 inch= 0.0254 m

(b): Bed containing RM –Al mixture

Fi g 4.4(a-b): Interstitial velocity against height of fluidized bed for different bed materials at different temperatures

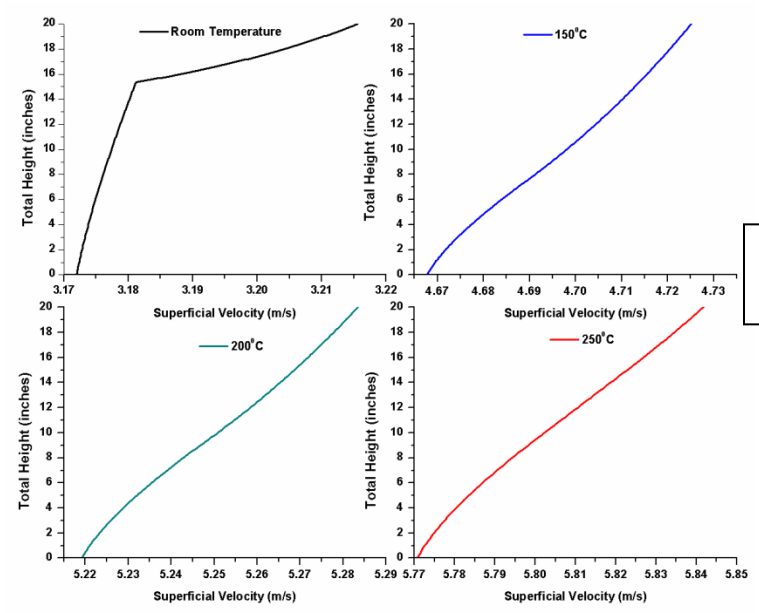

(a): Bed containing RM

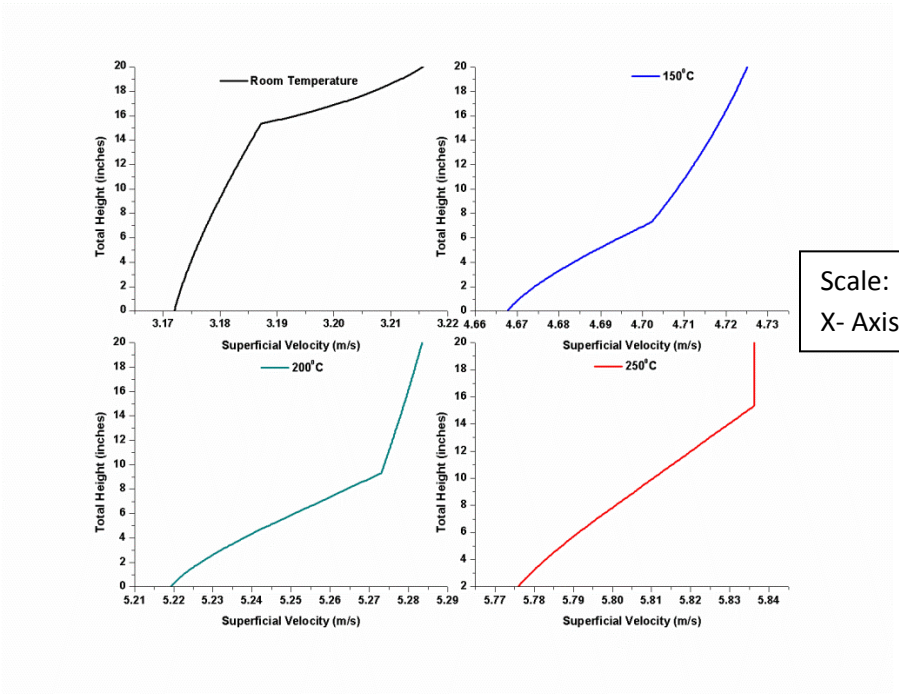

(b): Bed containing RM –Al mixture

Fig 4.5(a-b): Height of fluidized bed against Superficial velocity for different bed materials at different temperatures

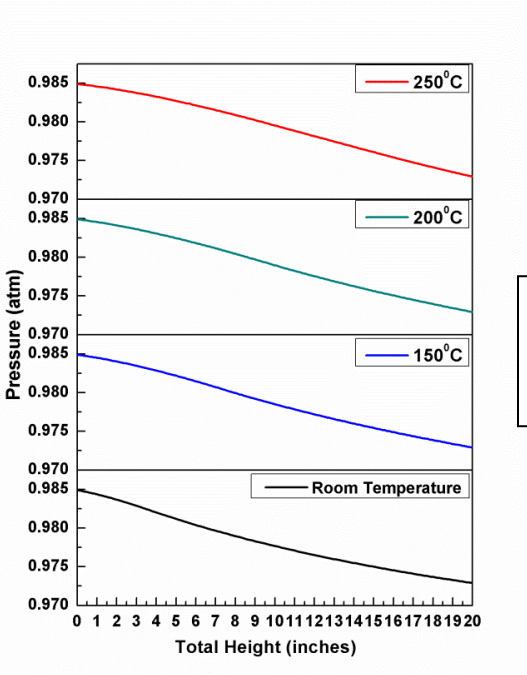

Scale:
X- Axis: 1 inch= 0.0254 m
Y-Axis: 1 atm = 101325 Pa

(a): Bed containing RM

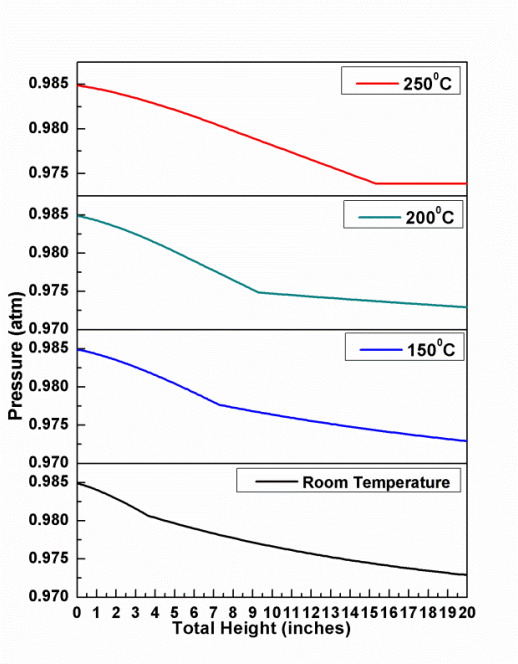

Scale:
X- Axis: 1 inch= 0.0254 m
Y-Axis: 1 atm = 101325 Pa

(b): Bed containing RM –Al mixture

Fig. 4.6 (a-b): Bed pressure against against height of fluidized bed for different bed materials at different temperatures

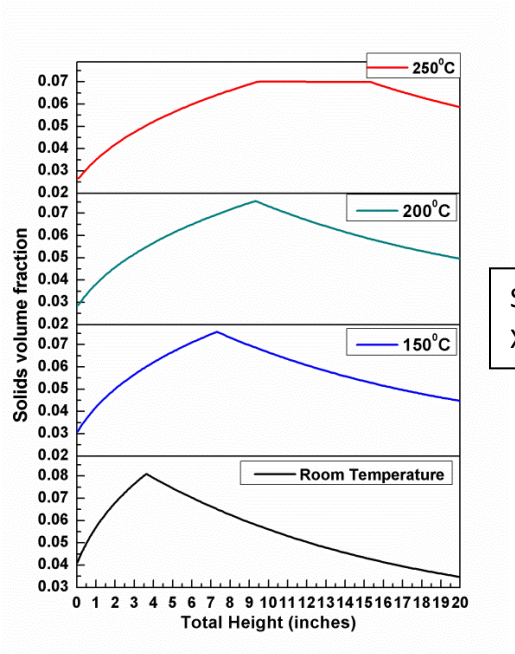

Scale:
X- Axis: 1 inch= 0.0254 m

(a): Bed containing RM

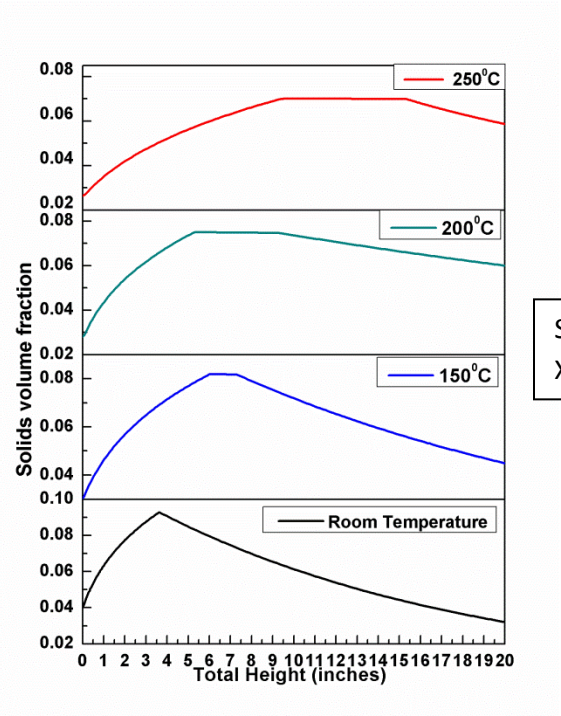

Scale:
X- Axis: 1 inch= 0.0254 m

(b): Bed containing RM –Al mixture

Fig 4.7 (a-b): Solid Volume Fraction against height of fluidized bed for different bed materials at different temperatures

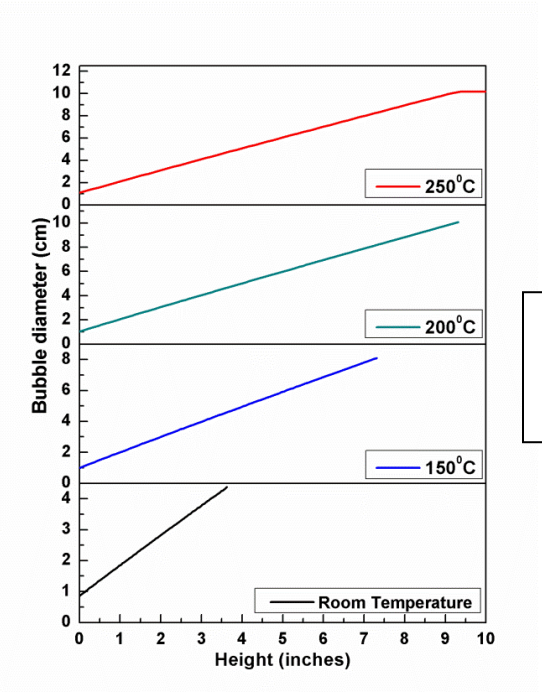

Scale:
X- Axis: 1 inch = 0.0254 m
Y-Axis: 1 cm = 0.01 m

(a): Bed containing RM

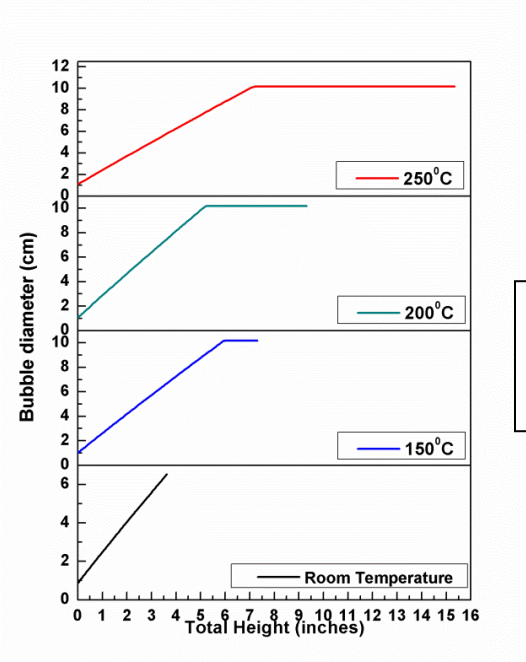

Scale:
X- Axis: 1 inch = 0.0254 m
Y-Axis: 1 cm = 0.01 m

(b): Bed containing RM –Al mixture

Fig 4.8 (a-b): Bubble diameter against height of fluidized bed for different bed materials at different temperatures

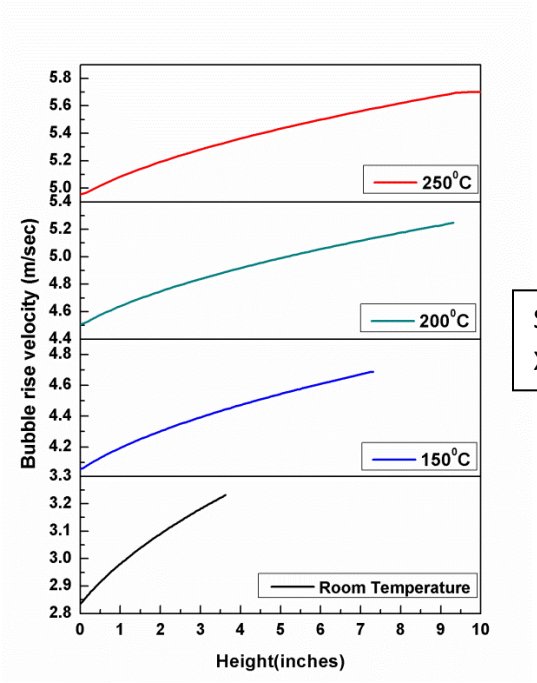

Scale:
X- Axis: 1 inch= 0.0254 m

(a): Bed containing RM

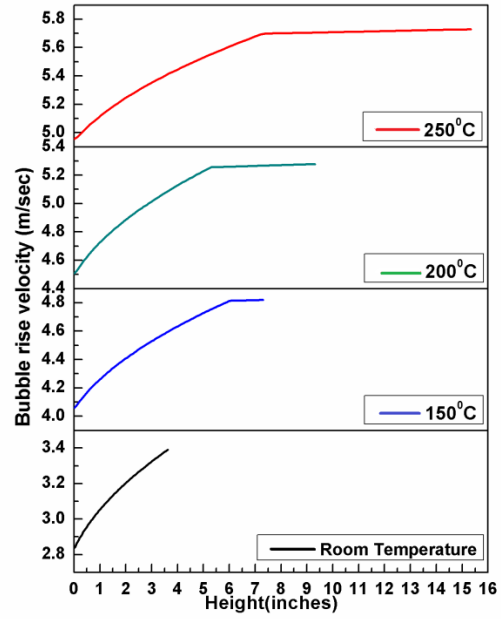

Scale:
X- Axis: 1 inch= 0.0254 m

(b): Bed containing RM –Al mixture

Fig.4.9 (a-b): Bubble rise velocity against height of fluidized bed for different bed materials at different temperatures

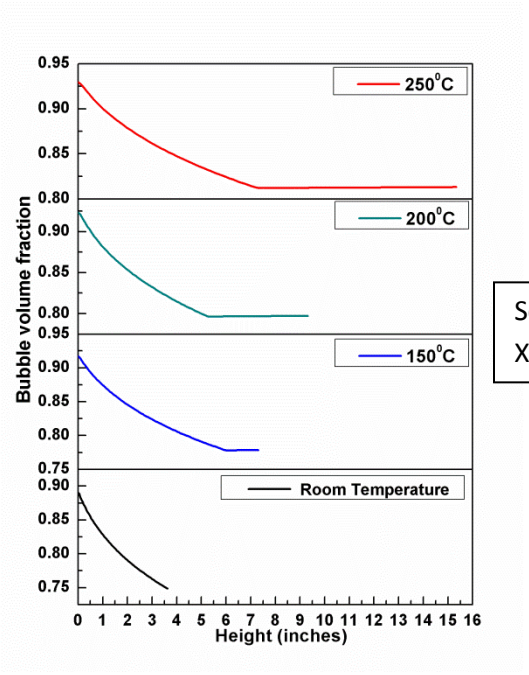

(a): Bed containing RM

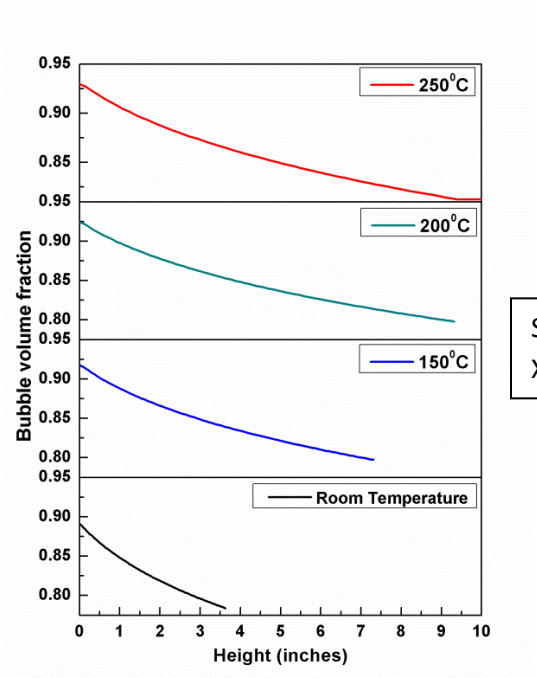

(b): Bed containing RM –Al mixture

Fig 4.10 (a-b): Bubble volume fraction against height of fluidized bed for different bed materials at different temperatures

CHAPTER – 5

RESULTS AND DISCUSSION

5.1 Analysis for RM as bed materials with and without effluent gas treatment

In order to carry the experiment, preliminary studies regarding the fluidization of the bed materials and its characterization is very important. As literature indicates that fluorides may react with metal particles at high temperature, it is essential to know the characteristics of RM (being the source of metal particles) at different temperatures for the present work. Depending upon the results obtained from the preliminary characterization of RM, the next step which consists of the reaction of the effluent gas with the bed materials is decided.

5.1.1 Fluidization Parameter

Fluidization is one of the best methods of providing proper fluid-solid contact. Different aspects affect the quality of fluidization. Again many aspects are to be analyzed as pre-requisites for proper fluidization. Minimum fluidization velocity is one of the aspects which is to be determined first. Preliminary experiments suggested that the RM particles of 77 microns ($77x10^{-6}$m) size have better fluidization quality and as such for our experiment the same has been considered as a bed material for the reaction. From Fig 5.1 it is found that the minimum fluidization velocity for particles of 77 microns ($77x10^{-6}$m) size is 0.014 m/s.

5.1.2. Heating Process

Fig.5.2 indicates the time taken by the FBR to reach the maximum temperature of 500^0C (773.15K). The reactor takes almost 26 minutes to attain a temperature of 150^0C (423.15K), 42 minutes to reach 200^0C (473.15K), 58 minutes to reach 250^0C (523.15K) and 147 minutes to reach 500^0C (773.15K).

5.1.3 XRD Analysis

Various researchers have studied the phase characterization and elemental analysis of RM but the data analysis for the composition of RM are found to be non-uniform because of its variation in elemental composition at different places. The XRD patterns of RM as observed at different temperatures are shown in Fig.5.3.From the XRD peaks of RM, it can be seen that the main components of the RM at room temperature are Hematite (α-Fe_2O_3), Calcite ($CaCO_3$), Gibbsite (γ-$Al(OH)_3$), Rulite (TiO_2), Sodium aluminum silicate ($Na(AlSiO_4)$), Dicalcium silicate (Ca_2SiO_4), and Quartz (SiO_2). Peaks of Tri calcium aluminate ($Ca_3Al_2O_6$) starts appearing for samples above 150^0C (423.15K). The XRD pattern of the elements are referred form JCPDS file of X'Pert HighScore software. Using peak broadening technique of X'Pert High Score software for XRD analysis, one can clearly differentiate the peaks. However with the compressed form of the graph, the analysis may not be very clear. Peaks of the sample treated at 500^0C (773.15K) shows that there is no Gibbsite in it. This may be due to that at 500^0C (773.15K) Gibbsite decomposes to Al_2O_3 and H_2O according to the following reaction

$$Al(OH)_3 \rightarrow Al_2O_3 + H_2O \qquad (1)$$

Literature shows that the above transformation takes place at temperatures above 600^0C (873.15 K) [62]. But in the present work the above transformation is found to occur at 500^0C (773.15K) which might have occurred due to proper heating of RM sample in the FBR. At 500^0C (773.15K) it is also found that Calcite ($CaCO_3$) starts decomposing to CaO and CO_2 [62] according to the following reaction.

$$CaCO_3 \rightarrow CaO + CO_2 \qquad (2)$$

Dicalcium silicate (Ca_2SiO_4) and hematite (α-Fe_2O_3) are not affected by the temperature through the process of heating. Thus the presence of these compounds in sample at 500^0C (773.15K) is confirmed by the peaks of XRD analysis.

5.1.4 Thermo gravimetric analysis (TGA)

The TGA-DTA diagram (Fig. 5.4) shows the thermal decomposition of RM. It is observed that as the temperature rises, there are three weight loss steps in the profile. The first one occurs at 25-260^0C (298.15K-533.15 K) where the weight loss is about 4.3 % of total weight which is due to the evaporation of water. The second step occurs in the temperature range of 260-325^0C (533.15-598.15 K) where weight loss is about 8.9% of total weight which is due to loss of H_2O from the sample as a whole and also removal of H_2O from $Al(OH)_3$. The third and the final step occurs in the temperature range of 325-500^0C (598.15-773.15 K) where weight loss is about 10.9% of total weight which may be due to the release of CO_2 during the decomposition of $CaCO_3$. The DTA curve shows two

broad peaks centered at around 60^{0}C (333.15K) and 290^{0}C (563.15), corresponding to the adsorption of water physically and chemically respectively [62].

5.1.5 Particle Size analysis (PSA)

The particle size is one of the most influential parameter for the fluidization process. The particle size is observed to undergo a significant change in size when the temperature increases. The particle size distribution of the RM at room temperature is shown in Fig.5.5. It can be seen that the sieved RM particles are mostly in the range of 0.137 microns ($0.137x10^{-6}$m) to 65 microns ($65x10^{-6}$m) with a mean value of 11.8 microns ($11.8x10^{-6}$m). But the size of the RM particles starts changing with the heat treatment inside the FBR, which is shown in Fig. 5.6. When the temperature reaches 150^{0}C (423.15K), the average particle size rises from 11.8 micons ($11.8x10^{-6}$m) to 18.1 microns ($18.1x10^{-6}$m) and then reaches 91.76 microns ($91.76x10^{-6}$m) at 200^{0}C (473.15K). The increase of the particle size may be influenced by the improvement in crystallization. From the XRD pattern (Fig.5.3), it can be seen that, except the vanishing phases like calcite and gibbsite, the crystallinities of the majority of phases of red mud are improved by heat treatment (e.g. Tri calcium aluminate) [62]. This promotes the rise in the value of the mean particle size. But as soon as the temperature reaches 250^{0}C (523.15K) the size of the particle decreases to 22.9 microns ($22.9x10^{-6}$m) and then decreases further to 19.1 microns ($19.1x10^{-6}$m) at 500^{0}C (773.15K). This is probably due to the inter-particle collision/impact/wear taking place inside the FBR leading to the reduction of particle size [34,62]. This may also be due to the formation of CO_2 as it behaves as a weak acid and helps in dissolution of larger particles [26, 62]. The variation of particle size at different temperatures is given in Table 5.1(a).

5.1.6. FESEM and EDX analysis

To study the phase change progress of RM during heat treatment inside FBR, known amount of the samples are dispersed in methanol and ultrasonicated for 30 minutes. Then the samples are observed under Field Emission Scanning Electron Microscopy to analyze the morphological structures of these samples. The FESEM images of RM sample observed at different temperatures are shown in Fig. 5.7(a-e). It can be seen from Fig. 5.7(a) that the arrangement of the particles is relatively loose or particles are poorly crystallized with high porosity and small particle size. On the contrary from Fig. 5.7(b) and Fig. 5.7(c) it can be observed that the RM treated at temperatures of 150^0 (423.15K) and 200^0C (473.15K) are increased in particle sizes. Again from the Fig.5.7 (d) and Fig.5.7 (e), it is found that at 250^0C (523.15K) and 500^0C (773.15K), particle size decreases which may be due to the attrition and collision effect of the particles inside the FBR thereby resulting in size reduction further. This increasing and decreasing trend is observed to be matching with the values measured by laser particle size analyzer. The EDX analysis of the respective samples ensures the presence of particular elements in it which is shown in Fig 5.8(a-e).

5.1.7. FT-IR analysis

The bands observed at different temperatures for different characterization groups are shown in Table 5.1(b). It is observed from Fig. 5.9 that broad bands occur at certain wave numbers for different samples. This may be due to the stretching vibrations of O-H bonds and H-O-H bending vibrations of interlayer adsorbed H_2O molecule [26,62]. Because of the large change in dipole moment of the water hydroxyl-stretching, the intensity of the infrared spectrum is more. But this bond is missing in case of IR curve for the sample

treated at 500^0C (773.15K) which may be due to the evaporation of moisture from the RM particles at that temperature. Stretching vibrations of C=O is found in the samples for a particular wave number confirms the presence of carbonate groups [26, 62]. The main reason being the presence of chemisorbed CO_2 in RM. Certain bands are observed for most of the RM samples which corresponds to the characteristic bands of Si-O and O-Si-O group as shown in Table 2 thereby confirming the presence of silicate groups. This group is absent in the RM sample treated at 500^0C (773.15K) temperature due to the dissolution of minerals like $Na(AlSiO_4)$ [26, 62]. Presence of Al^{3+}-O^{2-} bonds are observed in most of the samples. Minor stretching vibrations of Fe-O is also observed in most of the cases at the region around 440 cm^{-1} wave number, but it is not very clear when the comparison among the graphs are considered. Hence the FT-IR results support the evidence of phase change data of XRD.

5.1.8. BET analysis

For knowing the surface area of the RM sample, BET apparatus is used. The RM samples are out-gassed for about 2hrs at a temperature of 200^0C (473.15K). The surface area is observed to be 31.19 m^2/g, 31.24 m^2/g, 31.32 m^2/g, 31.39 m^2/g and 31.66m^2/g for RM samples at room temperature, 150^0C (423.15K), 200^0C (473.15K), 250^0C (523.15K) and 500^0C (773.15K) respectively. The increase in the surface area is matching with the decomposition of $Al(OH)_3$ phases of gibbsite. This may be due to the formation of small pores as free H_2O is removed from the sample when the temperature increases. It may also be due to the attrition or particle-particle collision effects which occur inside the FBR thus resulting in the breakage of the particles thereby exposing more surfaces.

5.2 Analysis for RM and RM-Al mixture as bed material with and without effluent gas

Analysis of bed materials after experiment was carried out for the two different bed materials (RM and RM-Al mixture). Industrial gaseous effluent was allowed to pass through these bed materials and residence time of 30 minutes was given so that the Fluorides present in the effluent gas react properly with the bed materials during fluidization process. After the experiments got over, the bed materials were analyzed again to compare the experimental results obtained before and after the reactions.

5.2.1 XRD Analysis:

XRD analysis of bed materials obtained after the reactions are shown in Fig. 5.10. From the Fig.5.3 of the bed materials before reaction, it is found that the XRD peaks of RM when fluidized at 250^{0}C (523.15K) contained Hematite (α-Fe_2O_3), Calcite ($CaCO_3$), Gibbsite (γ-$Al(OH)_3$), Rulite (TiO_2), Sodium aluminum silicate ($Na(AlSiO_4)$), Dicalcium silicate (Ca_2SiO_4), Quartz (SiO_2) and Tri calcium aluminate($Ca_3Al_2O_6$). In the current analysis i.e. after reaction minor peaks of Alumina (Al_2O_3) are observed which might have occurred because of the dissociation of Gibbsite into Alumina and water. Fig.5.10 shows the XRD patterns obtained after experiments with/without the effluent gas which are then compared with each other. The XRD peaks obtained for the Red Mud which was treated with the Effluent Gas at 250^{0}C (523.15K) was observed to contain Iron Di-Fluoride (FeF_2), Iron Tri-Fluoride (FeF_3) and minute peaks Aluminum Tri-Fluoride (AlF_3) and Sodium Fluoride (NaF), which may be due to the reaction of the fluorides present in the Effluent Gas with the Hematite (α-Fe_2O_3), Alumina (Al_2O_3) and Sodium Oxide (Na_2O) present in the Red Mud. The presence of these compounds in the Red Mud

sample after the experiment confirms the occurrence of the reaction thereby indicating the abatement of gaseous Fluorides by Red Mud in the FBR. In other experiment Red Mud mixed with Al powder was fluidized inside the FBR Industrial gaseous effluent was allowed to pass through the bed material and was allowed to react with the bed material maintaining all the above conditions and procedures, the XRD results of the samples shown in Fig. 5.10 are observed to contain Iron Di-Fluoride (FeF_2), Iron Tri-Fluoride (FeF_3), Aluminum Tri-Fluoride (AlF_3) and Sodium Fluoride (NaF). Here the Aluminum Tri-Fluoride (AlF_3) peak is more dominant which may be due to the addition of Aluminum powder to the red mud in the bed material. Aluminum Tri-Fluoride (AlF_3) might have formed by the reaction the bed materials (present in both red mud and added aluminum) and Fluorides present in the effluent gas. The peaks obtained in this case is observed to contain Aluminum (Al), Alumina (Al_2O_3), Hematite (α-Fe_2O_3), Calcite ($CaCO_3$), Gibbsite (γ-$Al(OH)_3$), Rulite (TiO_2), Sodium aluminum silicate ($Na(AlSiO_4)$), Dicalcium silicate (Ca_2SiO_4), Tri calcium aluminate($Ca_3Al_2O_6$) and Quartz (SiO_2) which are actually the Red Mud constituents. This analysis confirms the occurrence of reaction which is our objective.

5.2.2 ICP-MS Analysis:

Three samples of Red Mud, Red Mud treated with Effluent Gas and Red Mud mixed with Aluminum treated with the Effluent Gas are characterized using the ICP-MS analysis which gives the information about the amount of elements present in the samples (Table 5.2(a)). From Table 5.2(a) it is observed that apart from the basic mineralogical composition of Red Mud, various heavy metals are also present. The Quartz content is observed to be more in case of the Red Mud- Aluminum mixture when treated with the

Effluent Gas. This may be because of the presence of dust in the form of Quartz in the Aluminum powder. The Alumina percentage is observed to increase from 13.72% in Red Mud to 16.19% in Red Mud when it is treated with the Effluent Gas which may be due to the probable presence of minor amount of un-converted Gibbsite which got oxidized again by the fluidizing gas thereby leading to the more formation of Alumina. The third sample is found to contain the maximum amount of Alumina (37.41%) which may be due to the oxidation of Aluminum that is added with the Red Mud and also probably due to the reaction of un–converted Gibbsite with the Oxygen present in the fluidizing gas.The Hematite content in the Red Mud sample is found out to be 50.29 % which later decrease to 45.24 % when Red Mud is reacted with the Effluent Gas, the reason may be due to the reaction of iron oxides present in the Red Mud samples with the gaseous Fluorides. The third sample is found to be having Hematite percentage of about 47.51. This increase confirms the probability that in this experiment the Fluorides present in the gaseous stream is prone to get reacted more with the Aluminum which was added to the bed rather than reacting with the Iron content of RM Another significant change in composition of Red Mud is observed for the Sodium Oxide (Na_2O) where the decrease in its amount for the reacted samples confirms the probable reaction of Sodium Oxide with the Fluorides resulting in the formation of Sodium Fluorides (NaF). Some of the reactions involved with the Fluoride abatement are.

$Fe_2O_3+6HF \rightarrow 2FeF3 + 3H_2O$ (3) $Al_2O_3+ HF \rightarrow AlF_3 + H_2O$ (4)

$Na_2O + 2HF \rightarrow 2NaF + H_2O$ (5)

5.2.3 PSA Analysis:

The particle sizes of all the samples are calculated with the help of Particle Size Analyzer, the sizes of which are shown in Table 5.2(b). The samples whose particle sizes

are analyzed are Red Mud at 250^{0}C (523.15K), Aluminum at initial conditions, Aluminum fluidized at 250^{0}C (523.15K), Red Mud reacted with Effluent Gas at 250^{0}C (523.15K) and Red Mud Mixed-Aluminum mixture reacted with the Effluent Gas at 250^{0}C (523.15K). From the Table 5.2(b) and Fig.5.11 (a-c) it is observed that the Aluminum which was fluidized at 250^{0}C (523.15K) has an average particle size of 56.266 microns (52.66x10^{-6}m) The average particle size of Red Mud when reacted with the Effluent Gas is found to increase from 22.907 (22.907x10^{-6}m) microns to 38.390 microns (38.390x10^{-6}m) which might have occurred due to the formation of new species of Iron Di and Tri Fluorides, Aluminum Fluoride and Sodium Fluoride. In other observation it is also observed that Red Mud-Aluminum mixture when reacted with Effluent Gas attained an average particle size of 72.017 microns (72.017x10^{-6}m), the increase in the size again attributes to the probable formation of the above mentioned compounds.

5.3 Validation

The results obtained from ICP-MS Analysis and ASPEN PLUS simulation are compared in Table 5.3(a) and Table 5.3(b). From the above mentioned tables it is seen that the simulated data and the experimental results matches very well. The small difference or error is due to the assumptions which are considered while working with the ASPEN PLUS Simulation. This difference can be reduced further if the exact reaction kinetics of the reactions taking place in the FBR is known. The results thus obtained can provide a brief insight about the resemblance of the experimental value and simulated values which can play a vital role in the scale up of the reactor.

TABLES

Table 5.1(a).Variation of particle size at different temperatures.

RM Samples	Particle Size (microns)($x10^{-6}$m)		
	Minimum	Maximum	Average
Room Temperature	0.137	65.335	11.767
150^{0}C	0.177	82.5.640	18.072
200^{0}C	8.447	1451.500	91.796
250^{0}C	0.173	76.482.5	22.907
500^{0}C	0.179	71.159	19.084

Table 5.1(b).FT-IR bands observed at different temperatures.

Group Characterization	Wave number of RM samples (cm^{-1})				
	Room Temperature	150^{0}C	200^{0}C	250^{0}C	500^{0}C
O-H, H-O-H (Broad Bands)	2919.68	3003.92	3033.73	3002.68	-
C=O	1449.46	1452.68	1449.27	1451.9	-
Si-O	989.28	989.96	990.65	986.35	993.32
O-Si-O	534.60	536.55	547.0	544.87	-
Al-O	805.50	804.90	805.05	805.46	805.85
Fe-O	442.02	444.12	442.15	438.77	466.23

Table 5.2(a) ICP-MS analysis for the various reacted red mud samples and red mud & aluminum reacted samples

Elements %	Red Mud	Red Mud + E.Gas	Red Mud + Al + E.Gas
SiO_2	4.96	5.54	8.12
Al_2O_3	13.72	16.19	37.41
Fe_2O_3	50.29	45.24	47.51
TiO_2	5.08	5.83	5.31
CaO	0.32	0.71	0.59
MgO	0.094	0.112	0.133
Na_2O	4.62	3.94	2.73
K_2O	Not Found	0.04	0.544
S	0.064	0.062	0.109
P_2O_5	0.109	0.141	0.121
MnO	0.115	0.113	0.113
V	0.045	0.049	0.036
Cr	0.055	0.057	0.037
Co	Not Found	0.003	Not Found
Ni	0.005	0.005	0.0135
Cu	Not Found	Not Found	0.045
Zn	0.121	0.127	0.192
Pb	Not Found	0.007	0.023
Y	0.001	0.001	0.0008

Table 5.2(b) Variation of particle size for various samples at 250^{0}C.

Samples	Particle Size (microns) (x10^{-6}m)		
	Minimum	**Maximum**	**Average**
Red Mud at 250^{0}C	0.173	76.482.5	22.907
Aluminum fluidized at 250^{0}C	12.968	211.109	56.266
Red Mud + Effluent Gas at 250^{0}C	4.348	170.395	38.390
Red Mud Mixed + Alumnium + Effluent Gas Gas at 250^{0}C	5.070	291.459	72.017

Table 5.3(a) Comparison of experimental results and simulated results with respect to changes in the composition of bed material (Red Mud)

Elements	Experimental Result (%)	Simulated Result (%)	Difference
SiO_2	10.47	9.89	0.58
Al_2O_3	15.25	9.91	5.34
Fe_2O_3	10.04	10.02	0.02
Na_2O	14.72	13.73	0.99

Table 5.3(b) Comparison of experimental results and simulated results with respect to changes in the composition of bed material (Red Mud-aluminum mixture)

Elements	Experimental result (%)	Simulated result (%)	Difference (%)
SiO_2	38.92	35.01	3.91
Al_2O_3	64.26	41.48	22.78
Fe_2O_3	19.48	10.0	9.48
Na_2O	13.73	14.4	0.67

FIGURES

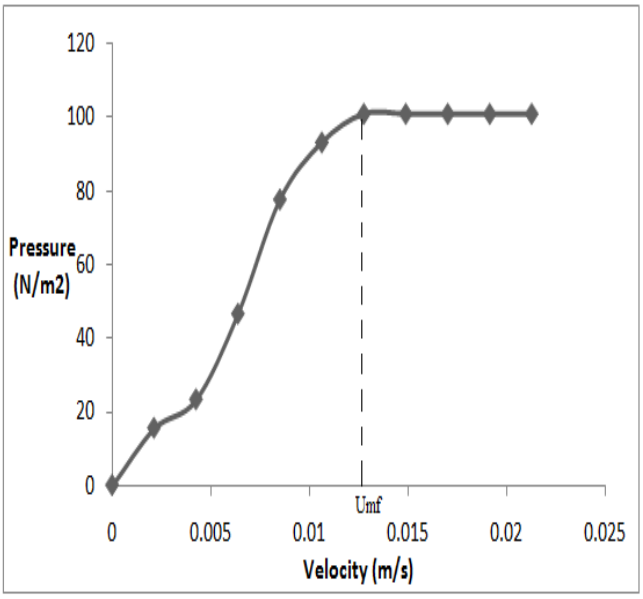

Fig 5.1 Pressure drop vs velocity plot for bed material (Red Mud) of 77 microns.

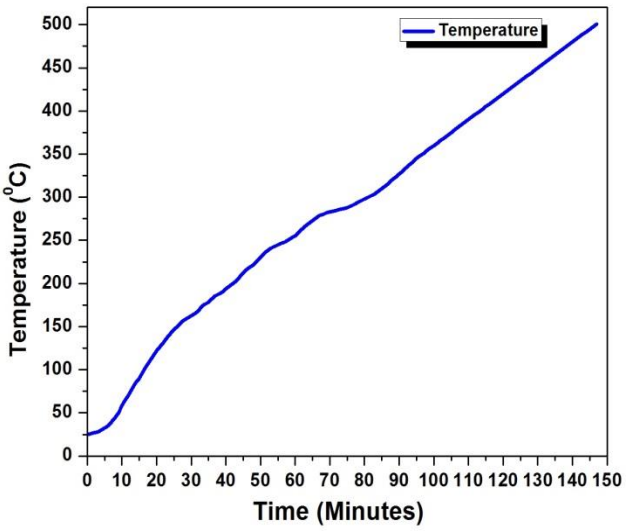

Fig 5.2 Heating curve of Red Mud

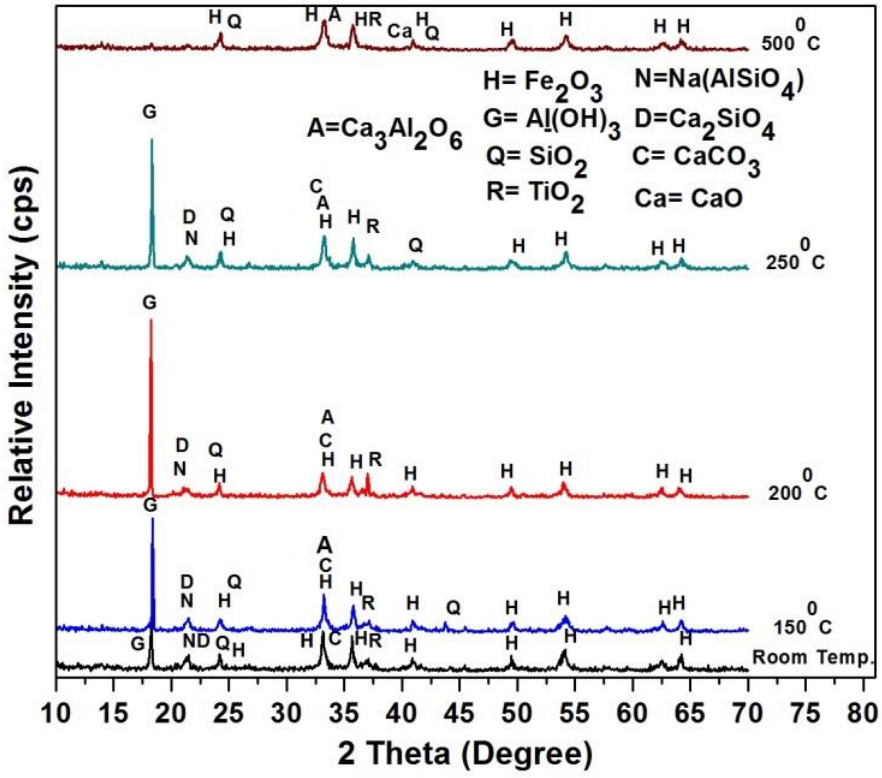

Fig 5.3 Comparison of XRD patterns of red mud at different temperatures

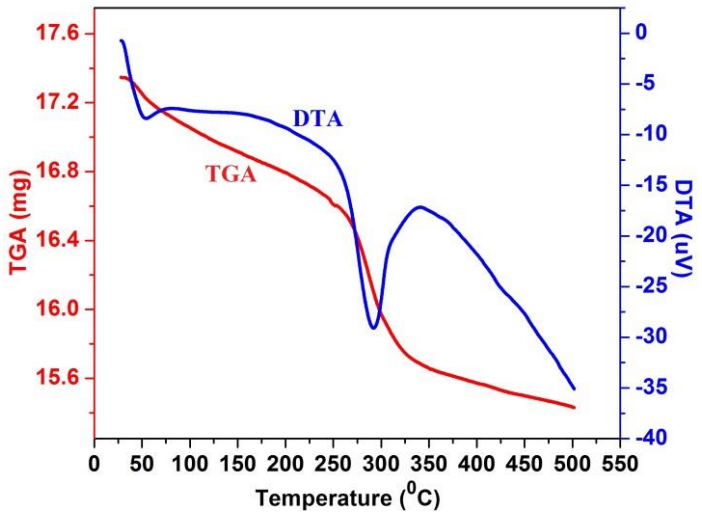

Fig 5.4TGA-DTA diagram showing weight loss of RM in the temperature range of 28°C to 500°C.

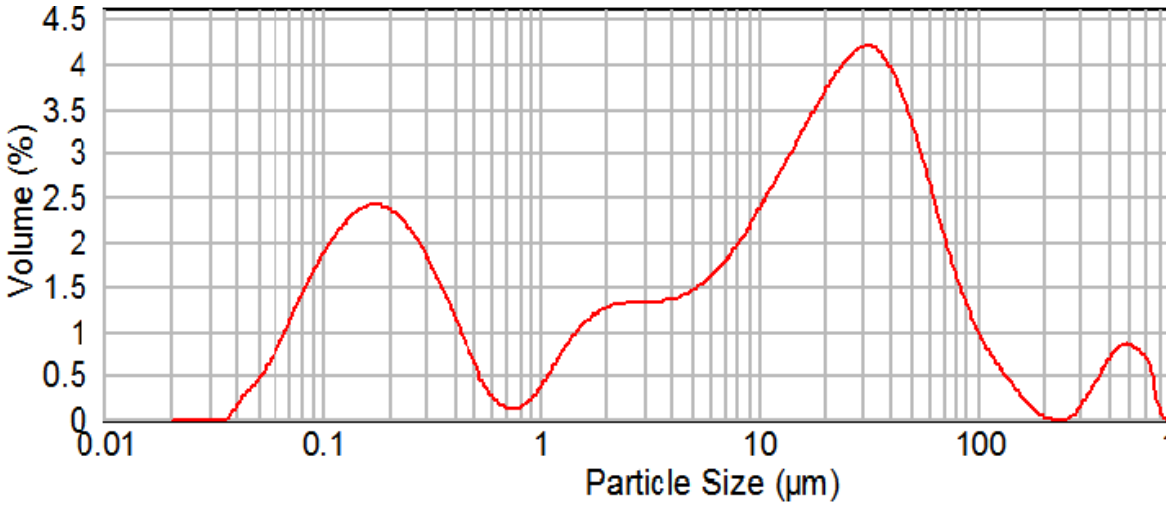

Fig 5.5 Particle size distribution of RM at room temperature

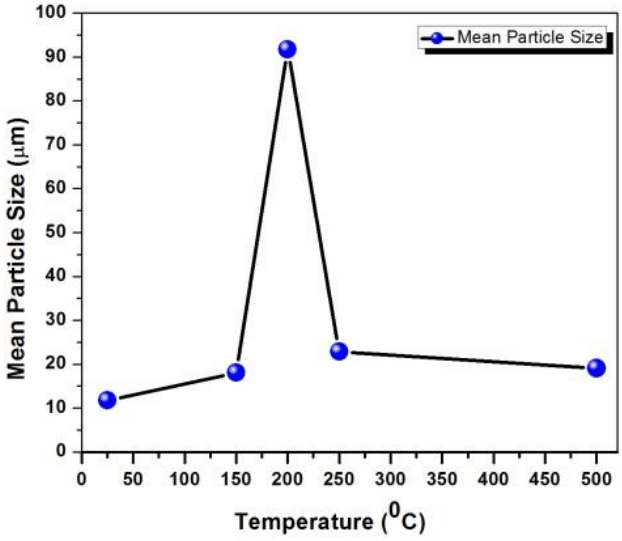

Fig 5.6 Particle size at different temperatures

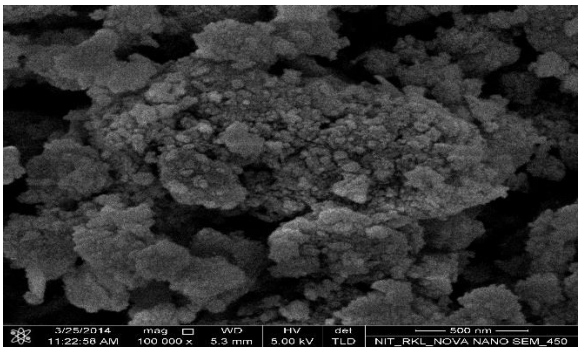

(a) Room Temperature

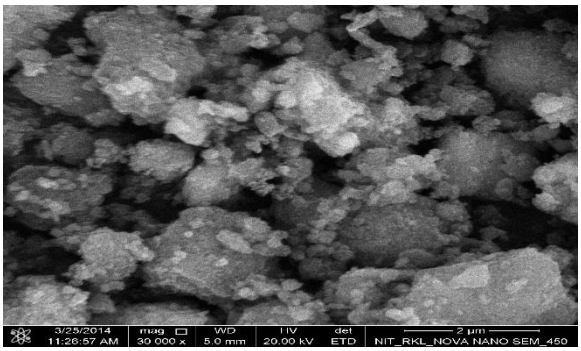

(b) 150^{0}C

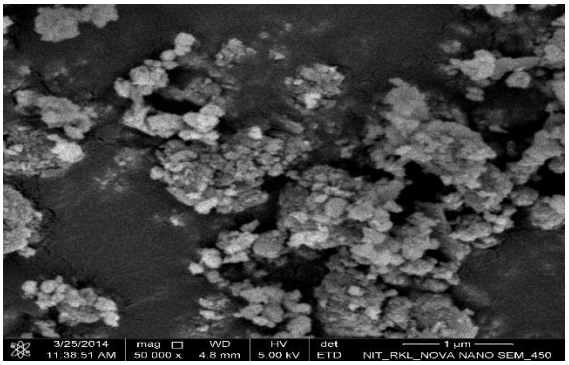

(c) 200^{0}C

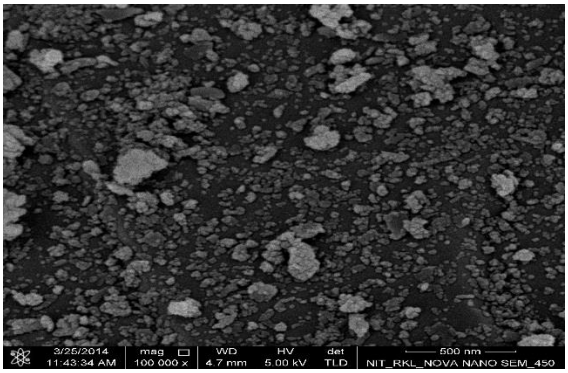

(d) 250 ^{0}C

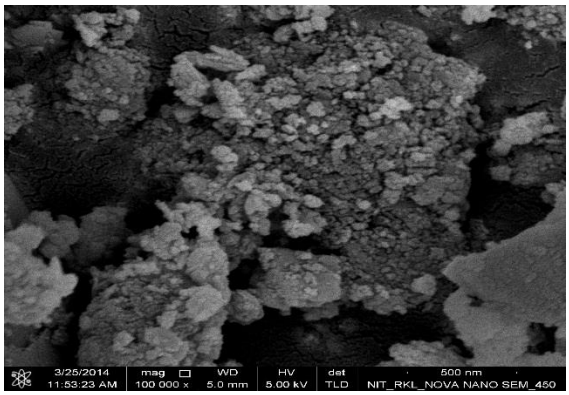

(e) 500^{0}C

Fig 5.7(a-e) FESEM images as observed at different temperatures

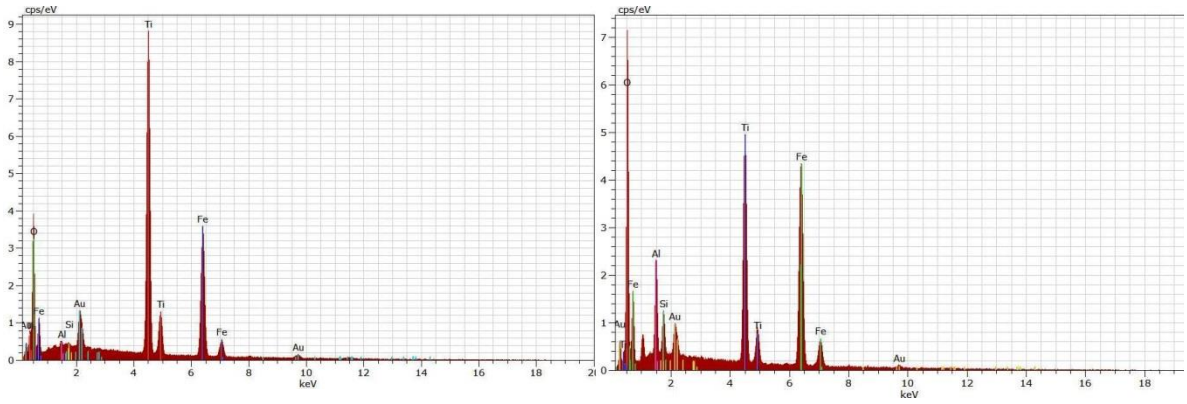

(a) Room Temperature **(b) 150^{0}C**

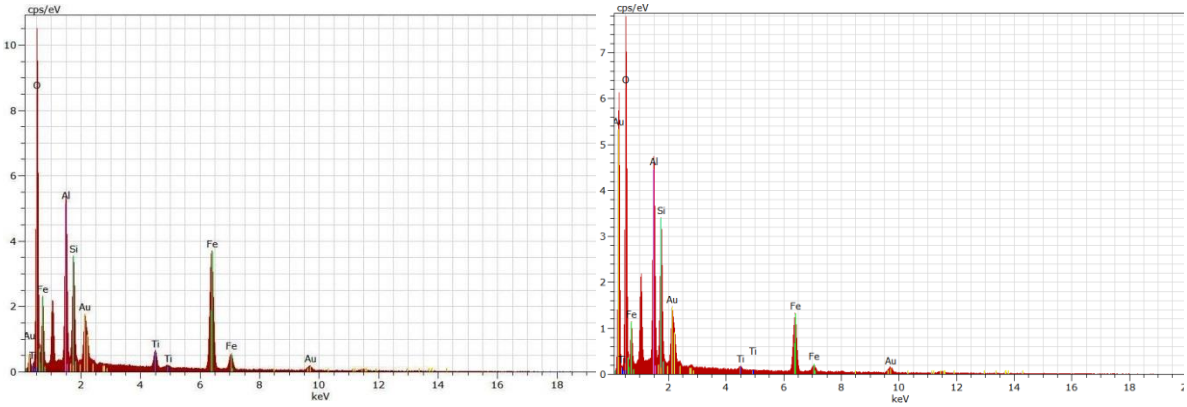

(c) 200^{0}C **(d) 250 ^{0}C**

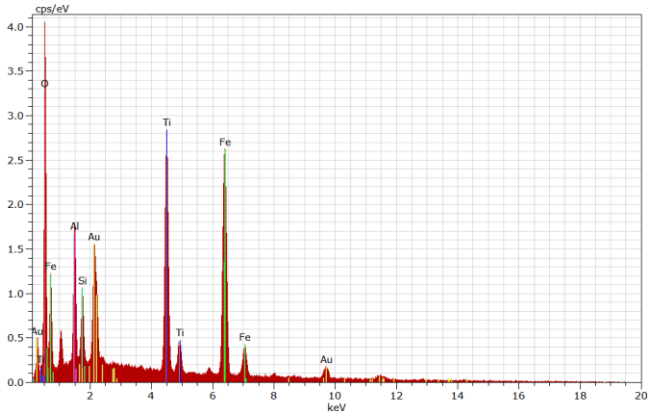

(e) 500^{0}C

Fig 5.8(a-e) EDX analysis for the samples as observed at different temperatures

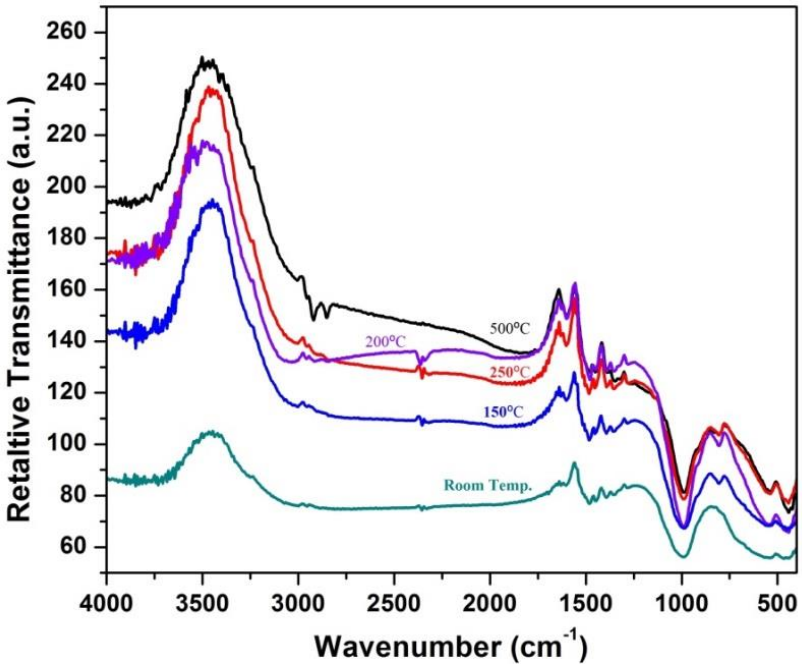

Fig 5.9 FT-IR spectra of RM at different temperatures

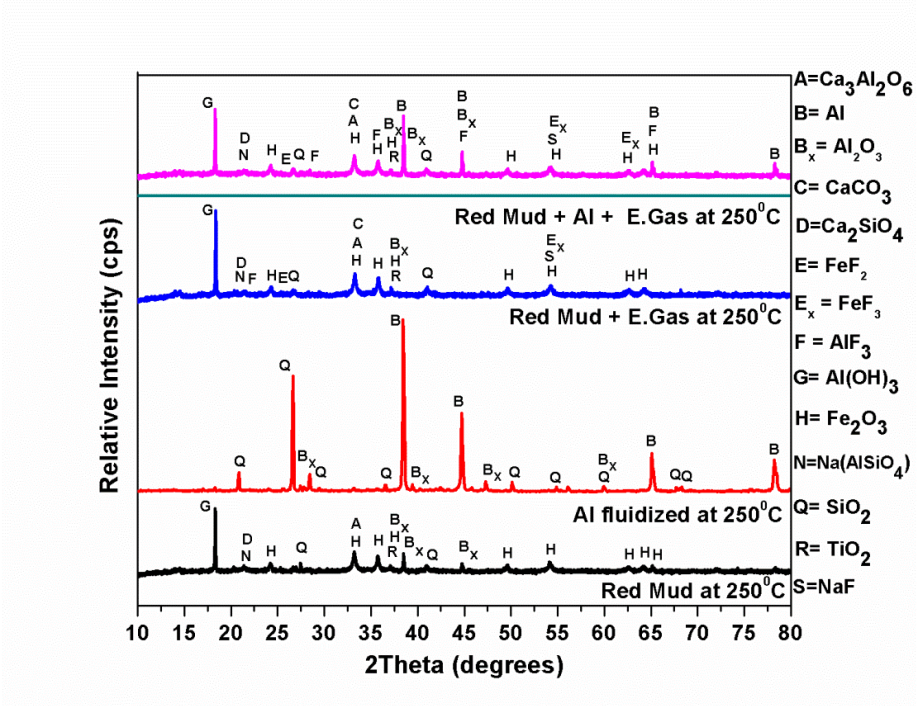

Fig 5.10 XRD patterns of RM when reacted with effluent gas (E.Gas) and RM-Al mixture when reacted with E.Gas at 250°C.

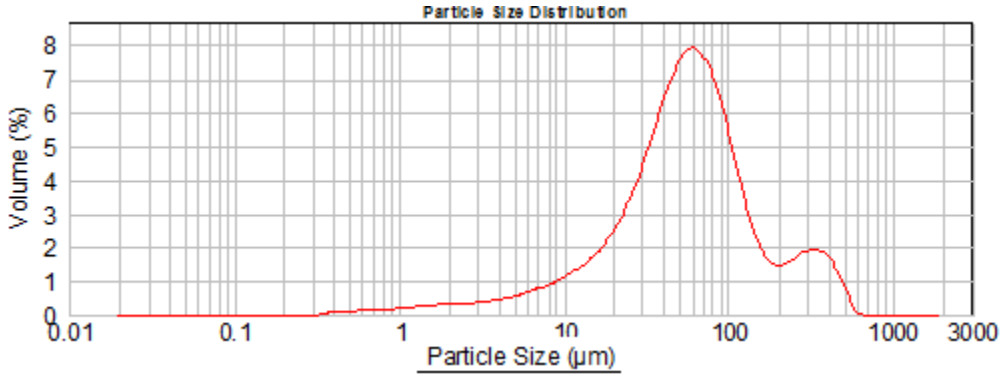

(a) Aluminum fluidized at 250^{0}C

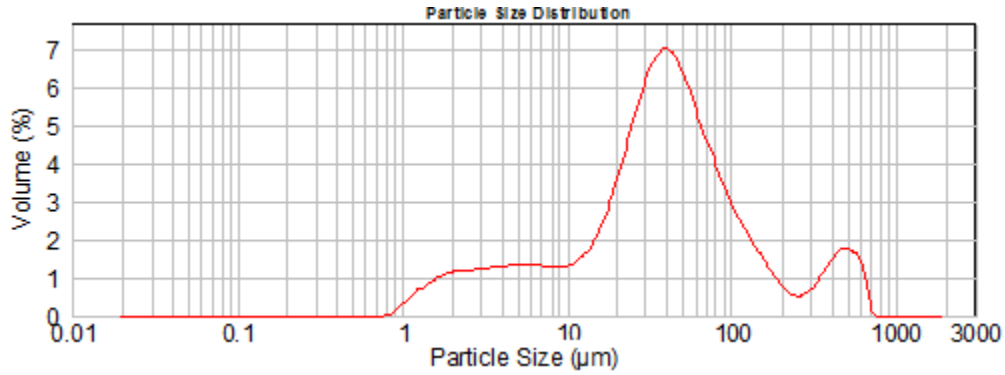

(b) RM when after reaction with effluent gas at 250^{0}C

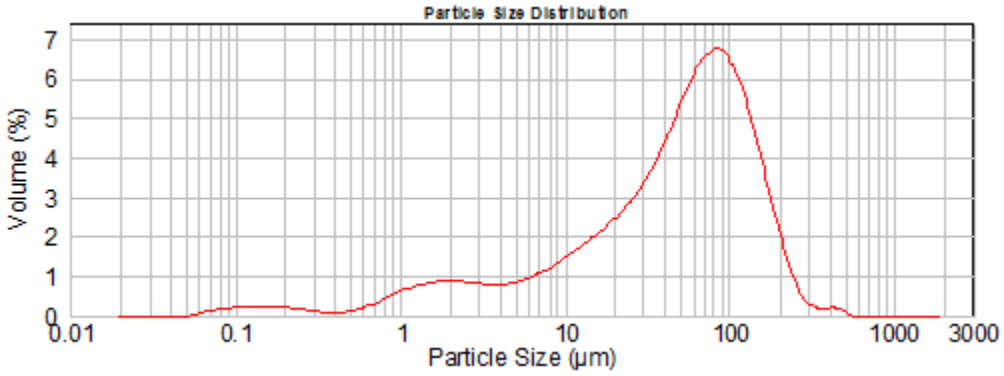

(c) Rm-Al mixture when reacted with effluent gas at 250^{0}C

Fig 5.11 Particle size distribution for various bed materials when fluidized at 250^{0}C

CHAPTER – 6

CONCLUSIONS

CONCLUSIONS

The bed hydrodynamics of a FBR have been studied the abatement of fluorides both experimentally and computationally using ASPEN PLUS Software.

Two sets of experiments were carried out in this study, first one where red mud ($77x10^{-6}$m)) is used as the bed material. In the second case red mud ($77x10^{-6}$m) and aluminum ($82.5x10^{-6}$m) mixture was used as the bed material. Experiments were carried out with and without the effluent gas for both the cases. When effluent gas was passed through the bed materials, fluorides present in the effluent gas reacted with metals presence in the bed materials. At higher temperatures the fluorides reacted with the various metallic oxides present in RM thereby forming various metallic fluorides. Maximum abatement was achieved for the second set where aluminum was used as an additional bed material to red mud. In the second set aluminum powder whose size is bigger than the RM powder samples were used in order to have better fluidization as well as to have better fluoride abatement due to the fact that the gaseous fluorides are more prone to react with direct metal when compared to the RM constituents. Thus it is observed that abatement of fluorides is around 25 % whereas it is only 10% with red mud only

Before using RM as a reactant, various mineralogical and phase transformation changes are studied using various characterization techniques. The products formed after the experiments were also studied using various instruments like XRD, ICP-MS etc. Due to the opaque nature of the FBR, the hydrodynamic studies were not visually possible hence ASPEN PLUS software was used. The simulation package also helped us in

studying the bed behavior at elevated temperatures as well as the product formation after the reaction. The results were validated well using this software.

Thus the experiments proved to be successful in order to achieve maximum abatement of harmful gaseous fluorides coming out from the aluminum industries by reacting it with its own waste called Red Mud which has practically got no market value. The results obtained from the simulation matches very well with the experimental results. This present work reveals that this technique i.e. use of red mud as bed material in a FBR can successfully be applied for other industries where fluoride emission is the major pollutant e.g. phosphatic fertilizer industries, semiconductor manufacturing industries etc. Therefore the scale up of the reactor as per the requirements of the industries can be achieved very easily using this study and can prove out to be a boon to all the industries which emit gaseous fluorides and especially aluminum industries which produce a huge amount of Red Mud as waste

6.1 SCOPE AND FUTURE WORK

- To study the various reaction kinetics occurring in the FBR leading to a better understanding and control of the reactions.
- Making the FBR more efficient by studying the various parameters such as residence time, bed PSD etc.
- Making the process more effective by proper insulation.
- Make use of the metallic fluorides in other useful processes.

ABBREVIATIONS

RM	:	Red Mud
Al	:	Aluminum
PSD	:	Particle Size Distribution
E.Gas	:	Effluent Gas (Obtained from Aluminum Industry)
XRD	:	X-Ray Diffraction
FT-IR	:	Fourier Transform Infrared Spectroscopy
FESEM	:	Field Emission Scanning Electron Microscope
EDX	:	Energy Dispersive X- Ray
BET	:	Brauner Emmit Teller
TGA	:	Thermo-gravimetric analysis
DTA	:	Differential Thermal Analysis
ICP-MS	:	Inductively Coupled Plasma- Mass Spectroscopy

REFERENCES

1) Mason B and Moore C B, Principles of geochemistry. 4th ed. New York: Wiley. 2004; 386–99.
2) Arno Jose I, Apparatus and process for the abatement of semiconductor manufacturing effluents containing fluorine gas. US Patent No.# 69056772007; April 18, 2000.
3) Jose L, Robert M. Fluorine abatement using steam injection in oxidation treatment of semiconductor manufacturing effluent gases. US Patent No.# 7407653; July 23, 2002.
4) Gary B, Delbert L, Amit K, Christopher L, Kenneth G. Rappe. Processes and apparatuses for treating halogen-containing gases. US Patent No.# 7407653; July 8, 2004.
5) Cady G H J, Reaction of Fluorine with Water and Hydroxides, Journal of American Chemical Society. 1935 ;(57): 246-249.
6) Vartanian V , Tonnis E, Graves D, Jewett R, Wofford B, Bevan J, Hartz C, Gunn M, Beu L and Lii T. Plasma Abatement Reduces PFC Emission. Semiconductor International. 2000; (23): 191-196.
7) Bohm E, Reh L, Weckesser E, Wilde G, Winkhaus G. Method of removing HF from gases. US Patent No.# 3907971 A; September 23, 1975.
8) Hsiung T H L , Withers Jr, Howard Paul (Breinigsville, PA). Abatement of F_2 using small particle fluidized bed. US Patent No.# 6,352,676; March 5, 2002.
9) L. Reh, in: P. Basu ŽEd. Circulating Fluidized Bed Technology. Pergamon, New York. 1986; 105
10) F. Ensgtrom, Y.Y. Lee, in: P. Basu, M. Horio, M. Hasatani ŽEds, Circulating Fluidized Bed Technology III. Pergamon, NY. 1991; 15.
11) Metso Automation Inc. Application report on Fluid Catalytic Cracking Unit, 2721/07/01 EN; December 2011.
12) Joris K , Martin J, André F. Development of fluidized bed combustion—An overview of trends, performance and cost. 2007; (33):ages 19–55
13) Heath T, Jukkola W, Lewis R, Malabre L, Smith D. Process of calcining alumina trihydrate in fluidized bed. US Patent No.# 2799558 A; July 16, 1957.

14) Renshui L. V-P-Si composite oxide catalyst precursor used for producing maleic anhydride from butance. US Patent No # 7547655 B2; June 16, 2009.

15) Vipin V, Paul $, Cottrell L. Process for the production of alkylaromatic hydrocarbons using solid catalysts. US Patent No.# 5012021 A; April 30, 1991.

16) Dennis J, Rear O, Steven S, Thomas V, Curtis L, Cong C. Preparation of high octane alkylate from Fischer-Tropsch Olefins. US Patent No.# 6743962 B2; June 1, 2004.

17) Rai S, Wasewar K, Mukhopadhyay J, Yoo C. and Uslu H. Neutralization and utilization of red mud for its better waste management. Archenviron Science. 2012; (6): 13-33.

18) Wang P, Lui D. Physical and Chemical Properties of Sintering Red Mud and Bayer Red Mud and the Implications for Beneficial Utilization, Materials. 2005; (5): 1800-1810.

19) Kalkan E. Utilization of red mud as a stabilization material for the preparation of clay liners. Engineering Geology. 2006 ;(87):220–229.

20) Wang S, Ang H M, Tade M O. Novel application of red mud as coagulant, adsorbent and catalyst for environmentally benign processes. Chemosphere. 2008 ;(72):1621–1782.5.

21) Sushil S, Batra VS. Catalytic applications of red mud, an aluminium industry waste: A review. Applied Catalysis B: Environmental. 2008; 81 (1-2):64-77.

22) Liu W, Yang J, Xiao B. Application of Bayer red mud for iron recovery and building material production from alumosilicate residues. Journal of Hazardous Materials. 2009;(161):474–478.

23) Amritphale S S, Anshul A, Chandra N, Ramakrishnan N, A novel process for making radiopaque materials using bauxite-Red mud. Journal of the European Ceramic Society. 2007 ;(27):1945–1951.

24) Pontikes Y, Nikolopoulos P, Angelopoulos GN, Thermal behaviour of clay mixtures with bauxite residue for the production of heavy-clay ceramics. Journal of the European Ceramic Society. 2007 ;(27):1645–1649.

25) Jeeshan K, Amritphale SS, Naveen C, Patel M. A novel binder free and energy efficient process for making ceramic tiles using red mud and sericitic pyrophyllite. Indian Journal of Chemical Technology. 2012; (19):420.

26) Xing G, Jiao Z Z. The development of non-autoclaved brick made of red mud and fly ash. Rare Metals Cemented Carbides. 1993; (6):154–177.

27) Pera J, Boumaza R, Ambroise J. Development of a pozzolanic pigment from red mud. Cement and Concrete Research. 1997;(27):1513–1522.

28) Vangelatos I, Angelopoulos GN, Boufounos D. Utilization of ferro-alumina as raw Material in the production of Ordinary Portland Cement. Journal of Hazardous Materials. 2009;(168):473–478.

29) Tsakiridis P E, Agatzini-Leonardou S, Oustadakis P. Red mud addition in the raw meal for the production of Portland cement clinker. Journal of Hazardous Materials. 2004; B116:103–110.

30) Singh M, Upadhayay SN, Prasad PM. Preparation of special cements from red mud.Waste Management. 1996;(8):665–670.

31) Kumar S, Kumar R, Bandopadhyay A, Innovative methodologies for the utilization of wastes from metallurgical and allied industries. Resources, Conservation and Recycling. 2006;(48):301–314.

32) Rai S, Wasewar KL, Mukhopadhyay J, Kyoo Yoo C, Uslu H. Neutralization andutilization of red mud for its better waste management; ARCH. ENVIRON. SCI. 2012;(6):13-33.

33) Dimas D D, Ioanna P, Panias D. Utilization of alumina red mud for synthesis of inorganic polymeric materials. Mineral processing and Extractive Metallurgy Review, 2009;30(3):211-239.

34) Qiu X R, Qi YY. Reasonable utilization of red mud in the cement industry (In Chinese). Cem. Technol. 2011; (6):103–105.

35) Nan XL, Zhang TA, Liu Y. Comprehensive utilization and analysis of Chinese red mud (In Chinese). Chin. J. Process Eng. 2010;(10):264–270.

36) Red mud Project. Available: http://www.redmud.org/Characteristics.html. May 02, 2005.

37) Agrawal A, Sahu KK, Pandy BD, Solid waste management in non-ferrous industries in India. Resources, Conservation and Recycling. 2004;(42):99–120.

38) Dong YL, Chuan-S. Stockpiling and Comprehensive Utilization of Red Mud Research Progress. Materials. 2012; (5); 1232-1246

39) Hajela R B, Gupta RG, Goel RK. Disposal of solid wastes—red mud and fly-ash in the production of heavy clay products. International Journal of Environmental Studies. 1989; 33(1,2):125-132.

40) Yang J K, Zhang D D, Xiao B, Wang X P. Study on glass-ceramics mostly made from red mud and fly ash (In Chinese). Glass Enamel. 2004;(32):9–11.

41) Wu B, Zhang D C, Zhang Z Z. The study of producing aerated-concrete blocks from red-mud (In Chinese). China Resour. Compr. Util. 2005;(6):29−31.

42) Qi J Z. Experimental Research on Road Materials of Red Mud; University of Huazhong Science and Technology: Wuhan, China; 2005.

43) Yang LG, Yao ZL, Bao DS. Pumped and cemented red mud slurry filling mining method (In Chinese). Mining Res. Develop. 1996;(16):18–22.

44) Traore D. L, Traore S, Diakite S. Bauxite Industry in Guinea and Value Opportunities of the Resulting Red Mud as Residue for Chemical and Civil Engineering Purposes. Journal of Civil Engineering Research. 2014; (1): 14-24.

45) Bekir Z, Inci A, Hayrettin Y. Sorption of SO2 on metal oxides in a fluidized bed. Ind. Eng.Chem. Res. 1988;(27):434–439.

46) Ciccu R, Ghiani M, Serci A, Fadda S, Peretti R, Zucca A. Heavy metal immobilization in the mining-contaminated soils using various industrial wastes. Miner. Eng. 2003;(16):187–192.

47) Pradhan J, Das SN, Thakur RS. Adsorption of hexavalent chromium from aqueous solution by using active red mud. Journal of Colloid and Interface Science. 1999 ;(217):137–141.

48) Liu X, Zhang N, Waste Management & Research. 2011; (29):1053-1077.

49) Vachon P, Tyagi RD, Auclair JC, Wilkinson KJ. Chemical and biological leaching of aluminum from red mud. Environmental Science and Technology. 1994;(28):26–30.

50) Snars K, Gilkes RJ. Evaluation of bauxite residues (red muds) of different origins for environmental applications. Applied Clay Science. 2009;(46):13–20.

51) Huang W, Shaobin W, Zhonghua Z, Li L, Xiangdong Y, Victor R et al.; Phosphate removal from wastewater using red mud; Journal of hazardous materials. 2008;(1):35-42.

52) Kunii D and Levenspiel O, "Fluidization Engineering", Second Ed., Butterworth-Heinemann, Boston, 1991.

53) Geldart D. "Types of gas fluidization". Powder technology 1973; (5): 285–292.

54) Aspen Technology, ASPEN PLUS user guide [M]. USA: Aspen Technology, 2000.

55) Weiss V, Fert F N, Helmerich H and Janssen K, Mathematical modelling of circulating Fluidized bed reactors by reference to solid decomposition reaction and coal combustion. Chem. Engg. Prog., 1987: (22); 79.

56) Basu P, Sett, A and Gbordzoe E.A.M., A simplified model for combustion of carbon in a circulating fluidized bed combustor, in FBC comes of Age, ed. J.P. Mustonen. ASME, New York. 1987; 738-742.

57) Y.Y. Lee, T. Hyppanen, in FBC Technology for Today, (Ed.: A.M. Manaker) ASME, New York, 1989 ;(82):53.

58) Young, B.E., Technico-economic evaluation of atmospheric fluidized bed combustion in steam production. M.Sc. A Thesis, Queen's University, Canada, 1986.

59) Paffenbarger, J., Analyse des Procedes a Lit Fluidise avaec ASPEN et USRFBC. CERCHAR, France, 1991.

60) Martin Fleer: Heat recovery from the Effluent Gas of aluminium reduction cells, MSc Thesis in Sustainable energy and engineering, Reykjavik University, January 2010.

61) Nath H, Sahoo A, "Abatement of fluorides using small particle fluidized bed", ICFCE-13, 2013, 288-293.

62) Campostrini R, Maurina S, Carturan G, Monagheddu M, Budroni G, CoccoG. Bauxite 'red mud' in the ceramic industry. Part 1: thermal behavior. Journal of the European Ceramic Society.2000; (20):235–244.

Powder Technology 269 (2015) 233–239

Contents lists available at ScienceDirect

Powder Technology

journal homepage: www.elsevier.com/locate/powtec

Characterization of Red Mud treated under high temperature fluidization

Harjeet Nath *, Pranati Sahoo, Abanti Sahoo

Department of Chemical Engineering, National Institute of Technology, Rourkela, India

ARTICLE INFO

Article history:
Received 12 June 2014
Received in revised form 1 September 2014
Accepted 4 September 2014
Available online 16 September 2014

Keywords:
Fluidized bed reactor
Minimum fluidization velocity
Particle size distribution
Red Mud

ABSTRACT

Red Mud (RM) is fluidized at different temperatures in a fluidized bed reactor (FBR). The phase composition and structural transition of RM fluidized at different temperatures are investigated. RM is treated in the FBR at different temperatures and above minimum fluidization velocity. The characteristic properties of RM treated in FBR at different temperatures are analyzed using XRD, TGA–DTA, PSA, FESEM, FT-IR and BET apparatus. It is observed that the different components of RM decompose on treatment of high temperature. The results thus obtained from RM treated at room and at higher temperatures are found to be much more promising where the temperature required for the decomposition of certain components is much less than the conventional heating methods. It is observed that gibbsite ($Al(OH)_3$) decomposes into Al_2O_3 & H_2O and calcite decomposes into CaO and CO_2 at higher temperatures. The particle size of treated RM is also analyzed where the particle size is found to increase initially and then decrease with the increase in temperature. The results obtained will thus provide an important base for the comprehensive utilization of RM for different applications.

1. Introduction

Red Mud (RM) is a reddish brown colored solid waste product produced in huge amounts from Aluminum Industries. The Bayer process is generally used in these industries for the digestion of bauxite ore in concentrated NaOH solution at appropriate temperature and pressure. During the digestion process aluminum reacts with NaOH to form soluble sodium aluminate leaving RM slurry as a waste [1]. It is reported that 0.8–1.5 tons of RM is generated per ton of alumina produced [2]. Globally 60–120 million tons of RM is produced annually and about 2 million tons of RM is produced in India itself [3]. The RM produced from these industries is generally stockpiled in open yard, which leads to serious problems in soil, air and water because it is highly caustic in nature [4]. The disposal of RM is now a major headache for the government for which researchers are currently working to develop suitable methods by which it can be utilized effectively. Thus the study of RM treatment and its utilization is very important and challenging.

Before working on RM for any use, it is essential to know its characteristics. The primary composition of RM is Al_2O_3 (17–20%), Fe_2O_3 (48–54%), SiO_2 (4–6%), TiO_2 (3–4%), Na_2O (3–5%), and CaO (1–2%) [5]. Various researchers are currently carrying out research work on RM treatment and utilization throughout the world. The researches include the recovery of important elements like Fe, Al, Na [6–8] and rare earth elements like Sc, Y, La, Ti, and V [8–12]. RM is now being used for cement production [13–16,32], brick production [17,18], glass production [19,20], aerated concrete blocks [21], filling material in mining [22,23], plastic [24], absorb heavy metallic ions like Cu^{2+}, Zn^{2+}, Ni^{2+}, and Cd^{2+} [25–27], removal of H_2S [28], removal of fluoride [29] and also for ceramic industry application [31].

Fluidized bed reactors are found to have huge applications in last few decades as compared to the fixed bed reactors and have become a versatile fluid–solid contacting device in chemical, bio-chemical, metallurgical and thermal power industries. The chief advantage lies in the fact that the solid particles get vigorously agitated in the bed by the fluidizing fluid passing through the bed thereby resulting in little or no temperature gradient even with highly endothermic and exothermic reactions [30].

For a better understanding of the physical and chemical properties of RM, the study of its behavior at higher temperature is very important. Various researches have already carried out researches to study the effect of temperature on the behavior of RM for knowing the physical and chemical properties where the RM samples were heated either inside an oven or inside a furnace or both [33,38], but the study of RM at higher temperatures inside a FBR is very much limited. Thus in this article focus is given to study the effect of temperature on characteristics of RM under fluidizing conditions. The research is supported by the characterization techniques such as XRD, TGA–DTA, particle size analyzer, FESEM and BET. This study provides an important base for the further studies on the behavior of RM inside a FBR.

2. Material and methods

2.1. Materials

The RM used in this study is collected from NALCO, Damanjodi, Odisha, India. The FBR used in this study is a cylindrical stainless steel

* Corresponding author at: Department of Chemical Engineering, NIT Rourkela, PIN: 769008, India. Tel.: +91 9692308349(M), fax: +91 6612472926.
E-mail address: harjeetnath@gmail.com (H. Nath).

http://dx.doi.org/10.1016/j.powtec.2014.09.011
0032-5910/

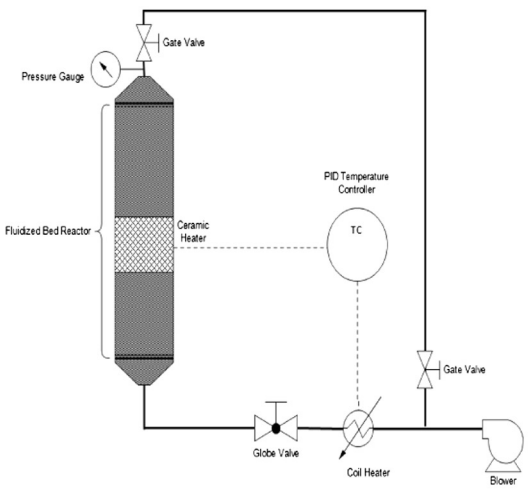

(a) Schematic view of the experimental setup

(b) Laboratory view of the experimental setup

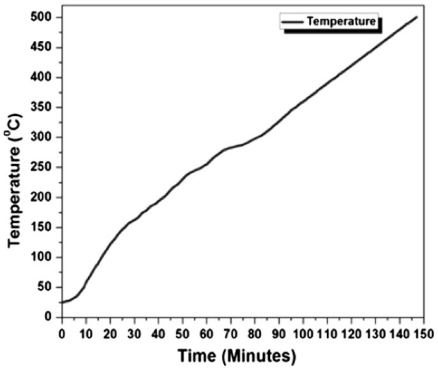

(c) Heating curve of Red Mudinside the FBR

Fig. 1. (a) Schematic view of the experimental setup. (b) Laboratory view of the experimental setup. (c) Heating curve of Red Mud inside the FBR.

shell of 10 cm internal diameter and 90 cm height. The experimental setup is as shown in Fig. 1(a) and (b).

2.2. Material preparation

The RM is produced in slurry form. On drying this slurry, lumps of RM are produced. The collected RM lumps are initially ground inside a ball mill and are then sieved. The average particle size of RM is found to be 77 μm by sieve analysis. 500 g of the sieved RM sample obtained is then taken in the FBR up to a certain height. The power supply is made on. The air flow is made through the blower. A heater is provided outside the FBR to maintain the bed temperature. The bed material is then made to fluidize just above the minimum fluidization velocity. The temperature is controlled by a PID controller and a temperature probe is inserted within the reactor by which inside temperature is noted. Four different samples are collected batch wise at fluidized temperatures of 150 °C, 200 °C, 250 °C and 500 °C and characterized by different methods. The observations are then compared with those of the samples fluidized at room temperature.

2.3. Heating process

The reactor takes almost 26 min to attain a temperature of 150 °C, 42 min to reach 200 °C, 58 min to reach 250 °C and 147 min to reach 500 °C. This temperature profile is shown in Fig. 1(c). At the attainment of the required temperatures, the reactor is opened and the sample is collected using a sample collector.

Table 1
List of apparatus.

Analysis	Equipment	Range
XRD analysis	Philips X'Pert X-Ray diffractometer	2θ range of 10° to 70° (spanning range of 3°min^{-1})
TGA analysis	Shimadzu DTG	28 °C to 500 °C (N_2 atmosphere)
Differential scanning calorimetry	Shimadzu DTG	28 °C to 500 °C (N_2 atmosphere)
Particle size	Malvern Mastersizer (Hydro 2000MU)	0.02 μ to 2000 μ
FESEM	Nova NanoSEM 450	–
EDX	Nova NanoSEM 450	–
FT-IR spectra	Perkin Elmer FT-IR Spectrometer (Spectrum RX-I)	4000–400 cm^{-1}
Surface area	BET (Quantachrome Autosorb-1)	–

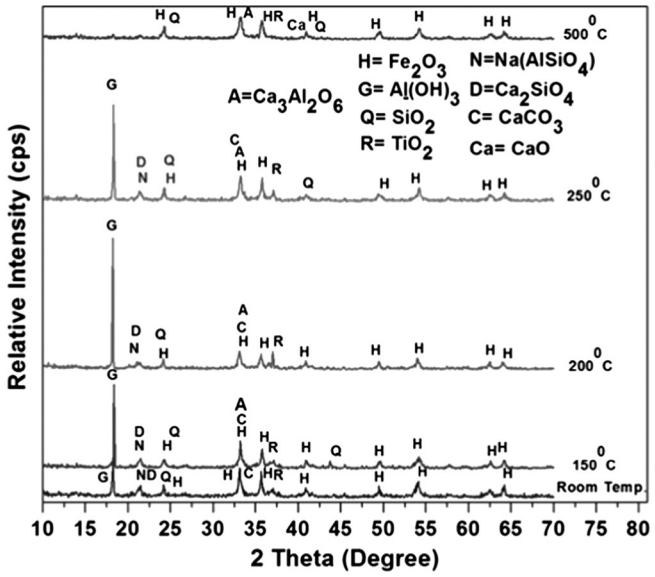

Fig. 2. XRD patterns of Red Mud at different temperatures.

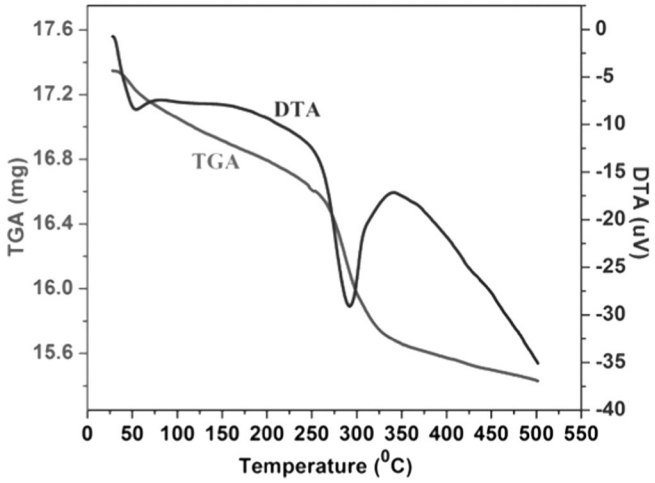

Fig. 3. TG–DTA diagram showing weight loss of RM in the temperature range of 28 °C to 500 °C.

2.4. Material characterization

The samples are collected at different temperatures i.e. room temperature, 150 °C, 200 °C, 250 °C and 500 °C. The reactor takes a total time of approximately 2.5 h to reach 500 °C. After fluidization the samples are collected and stored inside sealed plastic packets after the samples are cooled to room temperature. The XRD pattern of the material and the material composition is analyzed using Philips X'Pert X-Ray diffractometer with a Cu Kα radiation source in a 2θ range of 10° to 70° at spanning range of 3° min^{-1}. The TGA and DTA techniques are also carried out using Shimadzu DTG-60H. In this analysis 17.361 mg of the RM sample at room temperature is used. The sample is heated in an alumina crucible at a heating rate of 10 °C min^{-1} from 28 °C to 500 °C in N_2 atmosphere where the gas flow rate is 35 ml min^{-1}. The particle size of the RM samples is measured using Malvern Mastersizer (Hydro 2000MU) (range: 0.02 μ to 2000 μ). FESEM and Energy Dispersive X-Ray (EDX) are used to study the surface morphology and elemental composition of the samples respectively using Nova NanoSEM 450.

The FT-IR spectra of the samples are obtained by using Perkin Elmer FT-IR Spectrometer (Spectrum RX-I). The range is taken between 4000 and 400 cm^{-1}. Each of the RM sample is mixed with Anhydrous KBr and is then pressed at 10 tons/cm^2 pressure to make translucent tablets required for the recording of FT-IR spectra. The BET surface areas of the samples are also measured by Quantachrome Autosorb-1 using liquid N_2.

3. Results and discussion

The apparatus used for the characterization of RM is shown in Table 1 which is used for different analyses (i.e. XRD, TGA, PSA, FESEM, FTIR and BET) at different temperatures in the range from 25 °C (room temperature) to 500 °C.

3.1. XRD analysis

Various researchers have studied the phase characterization and elemental analysis of RM but the data analysis for the composition of RM is found to be non-uniform because of its variation in elemental composition at different places. The XRD patterns of RM as observed at different temperatures are shown in Fig. 2.

From the XRD peaks of RM, it can be seen that the main phases of the RM at room temperature are hematite (α-Fe_2O_3), calcite ($CaCO_3$), gibbsite (γ-$Al(OH)_3$), rulite (TiO_2), sodium aluminum silicate ($Na(AlSiO_4)$), dicalcium silicate (Ca_2SiO_4), and quartz (SiO_2). The peaks of tricalcium aluminate ($Ca_3Al_2O_6$) start appearing for samples above 150 °C. The XRD pattern of the elements is referred from JCPDS file of X'Pert High Score software. Using peak broadening technique of X'Pert High Score software for XRD analysis, one can clearly differentiate the peaks. However due to the compressed form of the graph, the analysis may not be very clear. The peaks of the sample treated at 500 °C show that there is no gibbsite in it. This is because gibbsite decomposes to Al_2O_3 and H_2O according to the following reaction

$$Al(OH)_3 \rightarrow Al_2O_3 + H_2O. \quad (1)$$

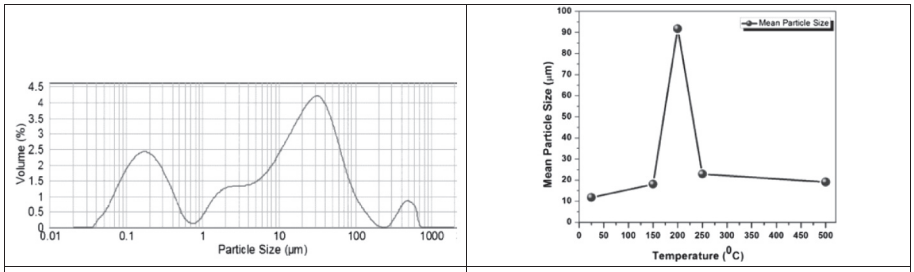

(a) Particle size distribution of RM at room temperature

(b) Particle size at different temperatures

Fig. 4. (a) Particle size distribution of RM at room temperature. (b) Particle size at different temperatures.

Table 2
Variation of particle size at different temperatures.

RM samples	Particle size (μm)		
	Minimum	Maximum	Average
Room temperature	0.137	65.335	11.767
150 °C	0.163	75.640	18.072
200 °C	8.447	1451.500	91.796
250 °C	0.173	76.475	22.907
500 °C	0.179	71.159	19.084

Literature shows that the above transformation takes place at temperatures above 600 °C [33]. But in the present work the above transformation was found to occur at 500 °C which might have occurred due to proper heating of RM sample in the FBR. At 500 °C it is also found that calcite ($CaCO_3$) starts decomposing to CaO and CO_2 [29] according to the following reaction.

$$CaCO_3 \rightarrow CaO + CO_2 \quad (2)$$

Dicalcium silicate (Ca_2SiO_4) and hematite (α-Fe_2O_3) are not affected by the temperature through the process of heating [33]. Thus the presence of these compounds in the sample at 500 °C is confirmed by the peaks of XRD analysis.

3.2. Thermogravimetric analysis (TGA)

The TGA–DTA diagram (Fig. 3) shows the thermal decomposition of RM. It is observed that as the temperature rises, there are three weight loss steps in the profile. The first one occurs at 25–260 °C where the

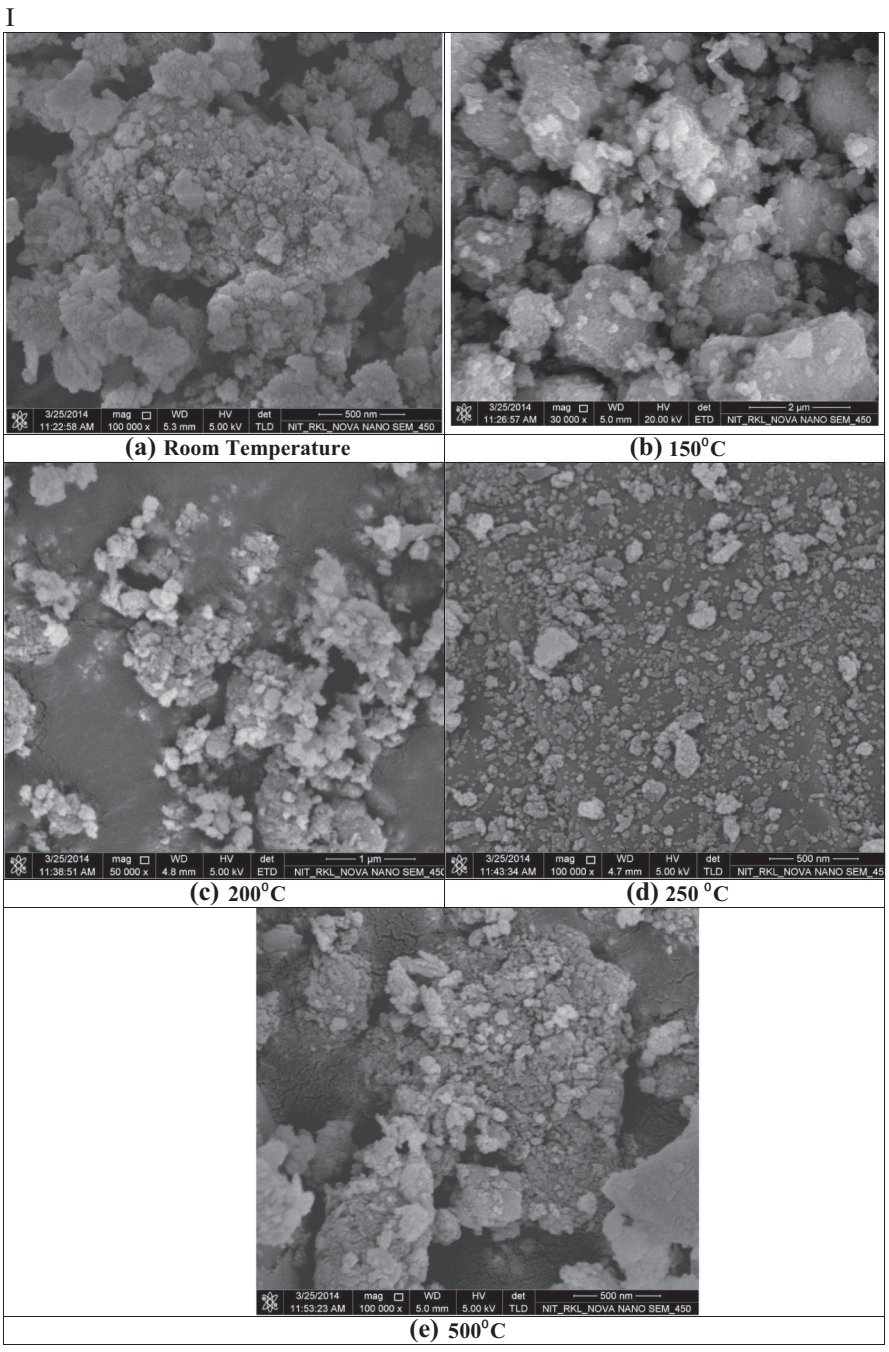

Fig. 5. I. (a–e) FESEM images as observed at different temperatures. II. (a–e) EDX analysis for the samples as observed at different temperatures.

II

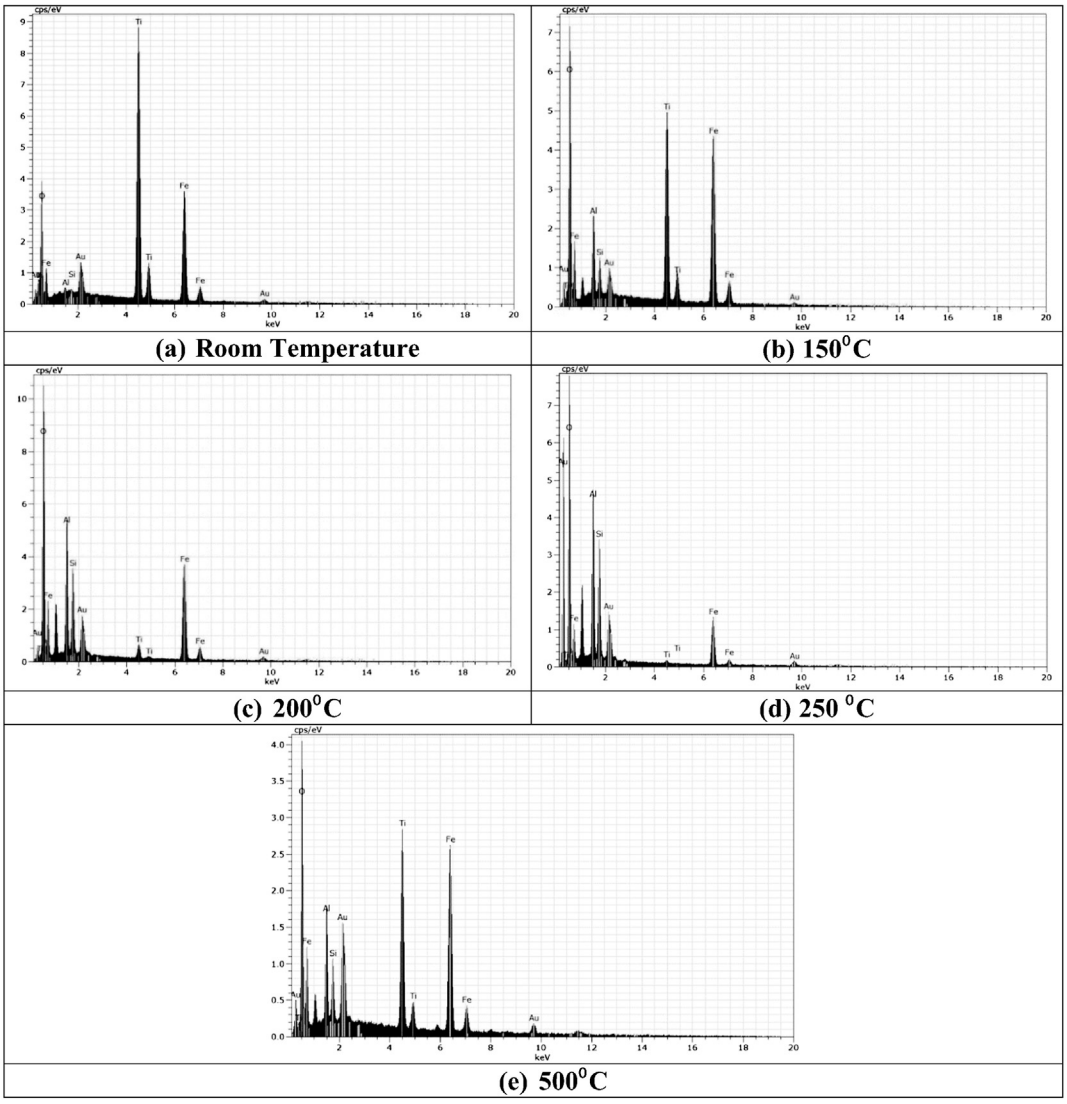

Fig. 5 (*continued*).

weight loss is about 4.3% of total weight which is due to the evaporation of water. The second step occurs in the temperature range of 260–325 °C where weight loss is about 8.9% of the total weight which is due to the loss of H_2O from the sample as a whole and also the removal of H_2O from $Al(OH)_3$. The third and the final step occurs in the temperature range of 325–500 °C where weight loss is about 10.9% of the total weight which may be due to the release of CO_2 during the decomposition of $CaCO_3$. The DTA curve shows two broad peaks centered at around 60 °C and 290 °C, corresponding to the adsorption of water physically and chemically respectively [34].

3.3. Particle size analysis (PSA)

The particle size is the most influential parameter for the fluidization process. The particle size is observed to undergo a significant change in size when the temperature increases. The particle size distribution of the RM at room temperature is shown in Fig. 4(a). It can be seen that the sieved RM particles are mostly in the range of 0.137 μm to 65 μm with a mean value of 11.8 μm. But the size of the RM particles starts changing with the heat treatment inside the FBR, which is shown in Fig. 4(b). When the temperature reaches 150 °C, the average particle size rises from 11.8 μm to 18.1 μm and then reaches 91.76 μm at 200 °C. The increase of the particle size may be influenced by the improvement in crystallization. From the XRD pattern (Fig. 2), it can be seen that, except the vanishing phases like calcite and gibbsite, the crystallinities of the majority of phases of RM are improved by heat treatment (e.g. tricalcium aluminate) [33]. This promotes the rise in the value of the mean particle size. But as soon as the temperature reaches 250 °C the size of the particle decreases to 22.9 μm and then decreases further to 19.1 μm at 500 °C. This is probably due to the inter-particle collision/impact/wear taking place inside the FBR leading to the reduction of particle size [35]. This may also be due to the formation of CO_2 as it behaves as a weak acid and helps in the dissolution of larger particles [36]. The variation of particle size at different temperatures is given in Table 2.

3.4. FESEM analysis

To study the phase change progress of RM during heat treatment inside FBR, known amount of the samples is dispersed in methanol and ultrasonicated for 30 min. Then the samples are observed under Field Emission Scanning Electron Microscopy to analyze the morphological structures of these samples. The FESEM images of RM sample observed at different temperatures are shown in Fig. 5-I(a), (b), (c), (d), and (e).

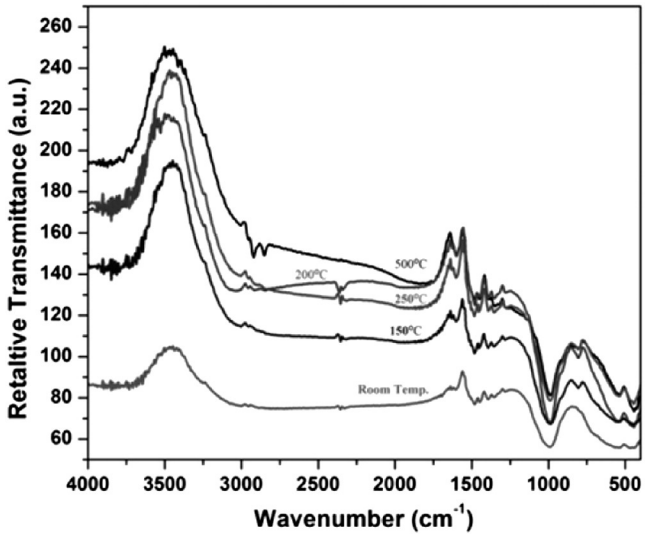

Fig. 6. FT-IR spectra of RM at different temperatures.

It can be seen from Fig. 5-I(a) that the arrangement of the particles is relatively loose or particles are poorly crystallized with high porosity and small particle size. On the contrary from Fig. 5-I(b) and (c) it can be observed that the RM treated at temperatures of 150° and 200 °C is increased in particle sizes. Again from Fig. 5-I(d) and (e), it is found that at 250 °C and 500 °C, particle size decreases which may be due to the attrition and collision effect of the particles inside the FBR thereby resulting in size reduction further. This increasing and decreasing trend is observed to be matching with the values measured by laser particle size analyzer. The EDX analysis of the respective samples ensures the presence of particular elements in it which is shown in Fig. 5-II(a), (b), (c), (d), and (e). From this figure the presence of elements like Fe, Al, Si and Ti is confirmed [36].

3.5. FT-IR analysis

The relative FT-IR spectrum of RM at different temperatures is shown in Fig. 6. The bands observed at different temperatures for different characterization groups are shown in Table 3. It is observed from Fig. 6. that broadbands occur at certain wave numbers for different samples. This may be due to the stretching vibrations of O – H bonds and H – O – H bending vibrations of interlayer adsorbed H_2O molecule [36]. Because of the large change in dipole moment of the water hydroxyl-stretching, the intensity of the infrared spectrum is higher. But this bond is missing in the case of IR curve for the sample treated at 500 °C which may be due to the evaporation of moisture from the RM particles at that temperature. The stretching vibrations of C═O found in all of the samples for a particular wave number confirm the presence of carbonate groups [37]. The main reason being the presence of chemisorbed CO_2 in RM. Certain bands are observed for most of the RM samples which correspond to the characteristic bands of Si – O and O – Si – O groups as shown in Table 3 thereby confirming the presence of silicate groups. This group is absent in the RM sample treated at 500 °C temperature due to the dissolution of minerals like $Na(AlSiO_4)$ [36]. The presence of $Al^{3+} - O^{2-}$ bonds is observed in most of the samples. Minor stretching vibrations of Fe – O are also observed in most of the cases at the region around 440 cm^{-1} wave number, but it is not very clear when the comparison among the graphs is being considered. Hence the FT-IR results support the evidence of phase change data of XRD.

Table 3
FT-IR bands observed at different temperatures.

Group characterization	Wave number of RM samples (cm^{-1})				
	Room temperature	150 °C	200 °C	250 °C	500 °C
O – H, H – O – H (broadbands)	2919.68	3003.92	3033.73	3002.68	–
C═O	1449.46	1452.68	1449.27	1451.9	1447.0
Si – O	989.28	989.96	990.65	986.35	993.32
O – Si – O	534.60	536.55	547.0	544.87	–
Al – O	805.50	804.90	805.05	805.46	–
Fe – O	442.02	444.12	442.15	438.63	466.23

3.6. BET analysis

For knowing the surface area of the RM sample, BET apparatus is used. The RM samples are out-gassed for about 2 h at a temperature of 200 °C. The surface area is observed to be 31.19 m^2/g, 31.24 m^2/g, 31.32 m^2/g, 31.39 m^2/g and 31.66 m^2/g for RM samples at room temperature, 150 °C, 200 °C, 250 °C and 500 °C respectively. The increase in the surface area is matching with the decomposition of $Al(OH)_3$ phases of gibbsite. This may be due to the formation of small pores as free H_2O which is removed from the sample when the temperature increases. It may also be due to the attrition or particle–particle collision effects which occur inside the FBR thus resulting in the breakage of the particles thereby exposing more surfaces.

4. Conclusions

In this work, the RM samples of 77 micron size are allowed to be heated up in a fluidized bed reactor, the fluidizing gas being an atmospheric air and the superficial velocity of air being little above the minimum fluidization velocity of RM particles. The samples are analyzed using XRD, TGA–DTA, PSA, FESEM, FT-IR and BET. The major phase changes observed are (i) gibbsite ($Al(OH)_3$) decomposes into Al_2O_3 and H_2O and (ii) calcite ($CaCO_3$) decomposes into CaO and CO_2. The temperatures required for these transformations are found to be less when compared to other conventional heat treatment methods. From the results of PSA and FESEM, it can be indicated that the particle size has a continuous rise up to 200 °C temperature because of the improvement of crystallinities of majority phases like tricalcium aluminate ($Ca_3Al_2O_6$), hematite (Fe_2O_3) etc. After that it decreased due to the particle–particle collision taking place inside the FBR which further resulted in the increase in the surface area of the samples. All the obtained data provide very much useful informations which can be used as an important base for the further studies of utilizing RM comprehensively.

Acknowledgments

The authors would like to thank the "(Ministry of Environment and Forests) (MoEF Sanction Order No. (103/118/2008-NT); Date: 15-02-2010), New Delhi, India" for the financial support. The authors also thank Prof. S.K. Sarangi, Director, NIT Rourkela for providing the necessary facilities.

References

[1] T. Newson, T. Dyer, C. Adam, S. Sharp, Effect of structure on the geotechnical properties of bauxite residue, J. Geotech. Eng. 132 (2) (2006) 143–151.
[2] X. Liu, N. Zhang, Waste Manag. Res. 29 (2011) 1053–1063.
[3] A. Agrawal, K.K. Sahu, B.D. Pandy, Solid waste management in non-ferrous industries in India, Resour. Conserv. Recycl. 42 (2004) 99–120.
[4] E. Fois, A. Lallai, G. Mura, Sulfur dioxide absorption in a bubbling reactor with suspensions of Bayer red mud, Ind. Eng. Chem. Res. 46 (2007) 6770–6776.
[5] M.J. Chaddha, S.B. Rai, R.N. Goyal, ENVICON 2007, National seminar on environmental concern and remedies in Alumina Industry at NALCO, Damanjodi, India, Characteristics of Red Mud of Indian Alumina Plants and Their Possible Utilization2007. 41–44 (2007).
[6] Y.F. Sun, F.Z. Dong, J.T. Liu, Technology for recovering iron from red mud by Bayer process, Metal Mine 9 (2009) 176–178 (Chinese).
[7] L. Zhong, Y.F. Zhang, Sub molten salt method recycling red mud, Chin. J. Nonferrous Metals 18 (2008) 70–73.
[8] X.F. Zheng, Recycling technology of aluminum and sodium from low temperature Bayer progress red mud, Shandong Metall. 32 (2010) 16–17.

[9] P.M. Orhsenkiihnn, T. Lybempudu, K.M. Ochsenkiihn, Recovery of lanthanides and yttrium from red mud by selective leaching, Anal. Chim. Acta. 319 (1996) 249–254.
[10] M. Ochsenkuhn-Petropulu, T. Lyberopulu, G. Parissakis, Selective separation and determination of scandium from yttrium and lanthanides in red mud by a combined ion exchange/solvent extraction method, Anal. Chim. Acta. 315 (1–2) (1995) 231–237.
[11] D.I. Smirnov, T.V. Molchanova, The investigation of sulphuric acid sorption recovery of scandium and uranium from the red mud of alumina production, Hydrometallurgy 45 (3) (1997) 249–259.
[12] X.H. Chen, Y. Chen, M. Gan, K.X. Xu, Precipitation and separation of vanadium frombayer process sodium aluminate solution, Chin. J. Process Eng. 10 (2010) 24–38.
[13] X.R. Qiu, Y.Y. Qi, The reasonable utilization of red mud in cement production, Cement Tech. 6 (2011) 103–105.
[14] E. Kalkan, Utilization of red mud as a stabilization material for the preparation of clay liners, Eng. Geol. 87 (3–4) (2006) 220–229.
[15] A.A. Barsherike, New Cement, in: Y.Y. Qian (Ed.), China Building Industry Press, Beijing, China, 1983.
[16] I. Vangelatos, G.N. Angelopoulos, D. Boufounos, Utilization of ferroalumina as raw material in the production of ordinary portland cement, J. Hazard. Mater. 168 (1) (2009) 473–478.
[17] A.P. Yang, The development of brick made of red mud and fly ash, Light Met. 12 (1996) 17–18.
[18] N. Yalcin, V. Sevinc, Utilization of bauxite waste in ceramic glazes, Ceram. Int. 26 (5) (2000) 485–493.
[19] J.K. Yang, D.D. Zhang, B. Xiao, Study on glass-ceramics mostly made from red mud and fly ash, Glass Enamel 32 (2004) 9–11 (Chinese).
[20] Z.Y. Liang, The research on black glass decorative materials made from red mud, Environ. Prot. Chem. Ind. 18 (1998) 50–51.
[21] B. Wu, D.C. Zhang, Z.Z. Zhang, The study of producing aerated-concrete blocks from red-mud, China Res. Compr. Util. 6 (2005) 29–31.
[22] L.G. Yang, Z.L. Yao, D.S. Bao, Pumped and cemented red mud slurry filling mining method, Min. Res. Dev. 16 (1996) 18–22.
[23] H.M. Wang, The comprehensive utilization of red mud, Shanxi Energy Conserv. 11 (2011) 58–61.
[24] X.L. Nan, T.A. Zhang, Y. Liu, Z.H. Dou, Analysis of comprehensive utilization of red mud in China, Chin. J. Process Eng. 10 (1) (2010) 264–270.
[25] M. Vaclavikova, P. Misaelides, G. Gallios, S. Jakabsky, S. Hredzak, Removal of cadmium, zinc, copper and lead by red mud, an iron oxides containing hydrometallurgical waste, Stud. Surf. Sci. Catal. 155 (2005) 517–525.
[26] M. Erdem, H.S. Altundogan, F. Tumen, Removal of hexavalent chromium by using heat-activated bauxite, Miner. Eng. 17 (2004) 1045–1052.
[27] L. Santona, P. Castaldi, P. Melis, Evaluation of the interaction mechanisms between red muds and heavy metals, J. Hazard. Mater. 136 (2) (2006) 324–329.
[28] R.C. Sahu, R.K. Patel, B.C. Ray, Removal of hydrogen sulfide using red mud at ambient conditions, Fuel Process. Technol. 92 (2011) 1587–1592.
[29] Y. Cengeloglu, E. Kır, M. Ersoz, Removal of fluoride from aqueous solution by using red mud, Sep. Purif. Technol. 28 (2002) 81–86.
[30] Y.K. Mohanty, B.P. Mohanty, G.K. Roy, K.C. Biswal, Effect of secondary fluidizing medium on hydrodynamics of gas–solid fluidized bed—statistical and ANN approaches, Chem. Eng. J. 148 (2009) 41–49.
[31] V.M. Sglavo, R. Campostrini, S. Maurina, et al., Bauxite "red mud" in the ceramic industry—part 1: thermal behaviour, J. Eur. Ceram. Soc. 20 (3) (2000) 235–244.
[32] X. Liu, N. Zhang, H. Sun, J. Zhang, L. Li, Structural investigation relating to the cementitious activity of bauxite residue—red mud, Cem. Concr. Res. 41 (8) (2011) 847–853.
[33] C.S. Wu, D.Y. Liu, Mineral phase and physical properties of red mud calcined at different temperatures, J. Nanomater. 2012 (2012), http://dx.doi.org/10.1155/2012/628592 (Article ID 628592, 6 pages).
[34] Y.N. Zhang, Z.H. Pan, Characterization of red mud thermally treated at different temperature, J. Jinan Univ. Sci. Tech. 19 (4) (2005) 293–297.
[35] S.M. Ivesona, J.D. Litster, K. Hapgood, B.J. Ennis, Nucleation, growth and breakage phenomena in agitated wet granulation processes: a review, Powder Technol. 117 (2001) 3–39.
[36] R.C. Sahu, R.K. Patel, B.C. Ray, Neutralization of red mud using CO_2 sequestration cycle, J. Hazard. Mater. 179 (2010) 28–34.
[37] C. Cardell, I. Guerra, J. Romero-Pastor, G. Cultrone, A. Rodriguez-Navarro, Innovative analytical methodology combining micro-X-ray diffraction, scanning electron microscopy-based mineral maps, and diffuse reflectance infrared Fourier transform spectroscopy to characterize archeological artifacts, Anal. Chem. 81 (2) (2009) 604–611.
[38] M.L.P. Antunes, S.J. Couperthwaite, F.T. Conceicao, C.P. Costa de Jesus, P.K. Kiyohara, A.C.V. Coelho, R.L. Frost, Red mud from Brazil: thermal behavior and physical properties, Ind. Eng. Chem. Res. 51 (2012) 775–779.